NAVAL POSTGRADUATE SCHOOL
Monterey, California

THESIS

NUMERICAL SIMULATION OF COLD SURGES

by

Nancy E. Harris

September 1985

Thesis Advisor: R.T. Williams

REPORT DOCUMENTATION PAGE

READ INSTRUCTIONS BEFORE COMPLETING FORM

1. REPORT NUMBER	2. GOVT ACCESSION NO. / 3. RECIPIENT'S CATALOG NUMBER
4. TITLE (and Subtitle): Numerical Simulation of Cold Surges	5. TYPE OF REPORT & PERIOD COVERED: Master's Thesis, September 1985
	6. PERFORMING ORG. REPORT NUMBER
7. AUTHOR(s): Nancy E. Harris	8. CONTRACT OR GRANT NUMBER(s)
9. PERFORMING ORGANIZATION NAME AND ADDRESS: Naval Postgraduate School, Monterey, California 93943-5100	10. PROGRAM ELEMENT, PROJECT, TASK AREA & WORK UNIT NUMBERS
11. CONTROLLING OFFICE NAME AND ADDRESS: Naval Postgraduate School, Monterey, California 93943-5100	12. REPORT DATE: September 1985
	13. NUMBER OF PAGES: 80
14. MONITORING AGENCY NAME & ADDRESS (if different from Controlling Office)	15. SECURITY CLASS. (of this report): Unclassified
	15a. DECLASSIFICATION/DOWNGRADING SCHEDULE

16. DISTRIBUTION STATEMENT (of this Report)

Approved for public release; distribution is unlimited

17. DISTRIBUTION STATEMENT (of the abstract entered in Block 20, if different from Report)

18. SUPPLEMENTARY NOTES

19. KEY WORDS (Continue on reverse side if necessary and identify by block number)

Numerical Weather Prediction; Numerical Simulation; Winter Monsoon; Monsoon Surge; Baroclinic Instability; Planetary Wave Forcing; Cold Surge

20. ABSTRACT (Continue on reverse side if necessary and identify by block number)

A global, six-level primitive equation model was numerically integrated to examine the interaction of a planetary wave with a growing mid-latitude baroclinic wave. The purpose of this study was to determine the contribution of the baroclinic wave to the initiation of a monsoon surge. Three experiments were run. Experiment I depicted the effect of the planetary wave on the southward migration of cold air. The cyclogenesis of a

#20 - ABSTRACT - CONTINUED

mid-latitude baroclinic wave was shown in Experiment II. Experiment III combined the growing baroclinic wave with the stable planetary wave in an attempt to simulate a cold surge. Characteristics of a monsoon surge were present in the numerical simulation but not to the extent or detail of observed surges. The results indicated the important role of planetary wave advections in the formation of cold surges.

Approved for public release; distribution is unlimited.

Numerical Simulation of Cold Surges

by

Nancy E. Harris
Captain, United States Air Force
B.S., State University of New York College at Brockport, 1975

Submitted in partial fulfillment of the
requirements for the degree of

MASTER OF SCIENCE IN METEOROLOGY

from the

NAVAL POSTGRADUATE SCHOOL
September 1985

ABSTRACT

A global, six-level primitive equation model was numerically integrated to examine the interaction of a planetary wave with a growing mid-latitude baroclinic wave. The purpose of this study was to determine the contribution of the baroclinic wave to the initiation of a monsoon surge. Three experiments were run. Experiment I depicted the effect of the planetary wave on the southward migration of cold air. The cyclogenesis of a mid-latitude baroclinic wave was shown in Experiment II. Experiment III combined the growing baroclinic wave with the stable planetary wave in an attempt to simulate a cold surge. Characteristics of a monsoon surge were present in the numerical simulation but not to the extent or detail of observed surges. The results indicated the important role of planetary wave advections in the formation of cold surges.

TABLE OF CONTENTS

LIST OF FIGURES

ACKNOWLEDGMENT

I owe a great debt of gratitude to everyone who supported me during my studies. Dr. R. Terry Williams deserves a special thanks for his patience, direction, support and assistance throughout this project. Much appreciation is also due to Dr. Mary Alice Rennick for her assistance with the numerical experiments, valuable insight into the results and review of the manuscript. I would also like to thank Capt. A. Shaffer for his indispensable help in running the UCLA model.

Several friends have greatly influenced me through my studies. Maj Jack Hayes was a strong supporter of my efforts. Jack's encouragement and assistance were immeasurable. A special note of thanks is extended to my tutors--Lt John Plenchner, Lt Cmdr Lee Devendorf and Capt Mary Jordan. I also want to say thank you to my husband and best friend, Wayne, for his understanding, support, encouragement and patience.

I. INTRODUCTION

The Asian winter monsoon has been an area of very active research over the past few years. Winter monsoons are dramatic manifestations of land-sea-air interaction. These phenomena consist of a mixture of all scales of motions, and the various interactions are still not well understood. Although the fundamental structure of the monsoon has frequently been observed, the dynamical mechanisms are still unknown. Recent areas of investigation include the role of the winter monsoon in mid-latitude tropical interaction, monsoonal variation and the forcing mechanisms for small scale monsoonal variations.

The monsoon is a three-dimensional, planetary scale wind regime which exhibits a strong seasonal dependence. It exhibits two distinct seasonal low-level wind flow patterns--a winter outflow from a cold continental anticyclone and a summer inflow into a continental heat low. The winter anticyclone and the summer heat low result from land-sea temperature differences and the varying position of the sun. The shapes of the continents and their topographies also play a role in producing the considerable regional and temporal variability of the monsoons.

Though centered far to the north, the Siberian anticyclone dominates the Southeast Asian winter (Ramage, 1971).

The low heat capacity of the land relative to the open ocean to the east and south ensures the development of the cold anticyclone with surface flow from land to ocean. A compensating flow from ocean to land occurs in the upper troposphere. The Himalayas block the southward movement of the extremely cold air from the Siberian anticyclone. As the anticyclone becomes established over Siberia, a surface cyclone develops over Indonesia and Malaysia as a major planetary scale convective area is shifted eastward from its summer position near India (Baker, 1983).

Chang and Lau (1980) analyzed the monthly mean velocity potential field at 200 mb for December 1974 and showed a broad region of divergence over Indonesia. This broad area of divergence is indicative of deep rising motions and large scale overturning in the atmosphere. A region of maximum convergence over northern China, in the vicinity of the Siberian anticyclone, was also noted.

A strong Hadley cell dominates the winter tropospheric circulation of this region. This thermally direct circulation involves the descent of cold air over the Siberian anticyclone, the southward flow of air at the surface, the ascent of warm air over Indonesia and a northward return flow at 200 mb.

Although the large scale features of the monsoon are identifiable from year to year, there is large interannual variability in strength and location. Velocity, temperature

and pressure fields vary on short time scales. One such variation is the monsoon surge, also known as the "cold surge." These events occur at intervals of several days to two weeks during the winter monsoon (Lim and Chang, 1981).

Observational studies by Danielson and Ho (1969), Chang et al. (1979), Murakami (1979), Chang and Lau (1980,1982) and Chang et al. (1983) discuss the characteristics and effects of the monsoon surge at the synoptic and planetary scales. The characteristics and effects described in these studies are summarized in the following paragraphs.

Over northern Asia there is intense, deep cold air advection associated with the passage of a mid-tropospheric trough. The trough intensifies rapidly over northern Japan. The baroclinicity increases with the anticyclogenesis over Siberia and cyclogenesis in the strong baroclinic zone off the east China coast. As the anticyclone intensifies, subsidence increases which strengthens the east Asian Hadley circulation. This intensification increases the upper-level ageostrophic flow, causing an acceleration of the east Asian subtropical jet near Japan.

The initiation of the monsoon surge occurs when the upper-level trough moves eastward and the pressure gradient along the east China coast increases. When the pressure gradient force exceeds the Coriolis force, the normal geostrophic balance is broken, resulting in cross-isobaric flow from high to low pressure. This accelerating northeasterly

low-level flow toward lower pressure is the monsoon surge. The surge reaches the equatorial South China Sea in 12-24 h. In the equatorial regions, convection intensifies within one to two days, sustaining the already enhanced Hadley circulation. The upper-level outflow from the convection accelerates eastward and westward along the equator as well as northward. The surge ends when the mid-latitude trough/ridge pattern moves far enough east, thus diminishing the strong subsidence over the anticyclone.

The monsoon surge has two stages separated by a few hours to one day depending on the location of the observing site (Lim and Chang, 1981; Chang et al., 1983). The pres-surge surge is the first stage. It is the leading edge of the downward accelerating air with a propagation speed characteristic of internal gravity waves. A frontal passage is the second stage which moves with advective speeds and is defined by a sharp decrease in surface dewpoint.

The cause or nature of monsoon surge forcing has been examined by Lim and Chang (1981) and Baker (1983). Linearized shallow-water equations on an equatorial beta-plane were used by Lim and Chang (1981) in an analytical study of monsoon response to simulated anticyclogenesis. They suggested that the large features of synoptic scale motions in the east Asian winter monsoon could be explained by pressure forcing using equatorial beta-plane dynamics. No consideration was given to orography, a variable mean zonal

wind, the vertical structure of monsoon surges or the upper tropospheric response to the surge.

Baker (1983) used a global, six-level primitive equation model to examine the interaction of a mid-latitude baroclinic wave with topography. A well-developed baroclinic wave could initiate a monsoon surge, however, the surges were weak with limited extent. Baker (1983) concluded that other forcing mechanisms were required to simulate the surges observed during the winter monsoon.

Shaffer et al. (1984) have shown that cold surge events are frequently preceded by rapid growth in the planetary waves. It appears that the amplified planetary wave helps advect the cold air toward the equator. The purpose of this study is to examine the interaction of a planetary wave with a growing baroclinic wave. The simulations will be carried out with a global, six-level primitive equation model. The same baroclinic jet will be used, as was employed by Baker (1983). The baroclinic wave, which is unstable with the jet, will have wave number 8. The planetary wave will be represented by wave number 4, which is stable with the jet.

II. DESCRIPTION OF MODEL

A version of the UCLA potential enstrophy conserving general circulation model is used in these experiments. The atmosphere is adiabatic, dry and frictionless. The governing equations of the model are the primitive equations (listed in Appendix A). The model design and dynamic processes are described by Arakawa and Lamb (1977,1981). The version used for these experiments is summarized below.

A. THE HORIZONTAL GRID

Arakawa's scheme C is used. The prognostic variables--wind (u,v), potential temperature (σ) and terrain pressure (π)--are staggered horizontally as shown in Figure 2.1. This

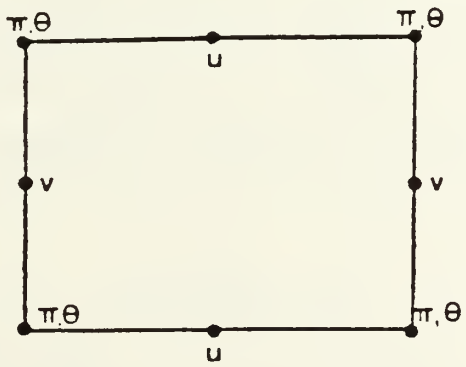

Figure 2.1. Horizontal distribution of variables in the UCLA model grid (Arakawa and Lamb, 1977).

grid arrangement requires more computer time than an unstaggered grid, but it provides a much better structure for the

shorter waves arising from geostrophic adjustment, smaller scale heating, nonlinear interaction or topographic effects. Grid resolution is 2.5° longitude by 4.0° latitude. A 90° sector of the globe extending from pole to pole is used as the computational domain. Cyclic continuity is imposed at the east and west boundaries.

Convergence of the meridians toward the poles normally requires a very short time step to ensure computational stability. Instead of shortening the time step, longitudinal averaging is done on the terms governing gravity wave propagation (Arakawa and Lamb, 1977). The averaging is done by expanding the zonal pressure gradient and zonal mass flux into a Fourier series around each latitude circle. The amplitude of each wave component is then reduced by the factor S. The gradients of the meteorological fields are smoothed instead of their Fourier expansions. Application of the smoothing operator, S, occurs at high latitudes where $S < 1$. The smoothing operator is defined as:

$$S = \frac{\Delta\lambda}{\Delta\phi} \frac{\cos\phi}{\sin(m\Delta\lambda/2)} \qquad (2.1)$$

(A list of symbol definitions is contained in Appendix B.)

B. THE VERTICAL GRID

The model equations are written using the vertical sigma coordinate:

$$\sigma = \frac{p - p_t}{\Pi} \qquad (2.2)$$

where:

$$\Pi = p_s - p_t.$$

p_s is the surface pressure, and p_t is the pressure at the top of the model atmosphere (p_t = 200 mb). The variables are vertically staggered in six equally spaced sigma layers (Figure 2.2). The surface and terrain pressure are defined

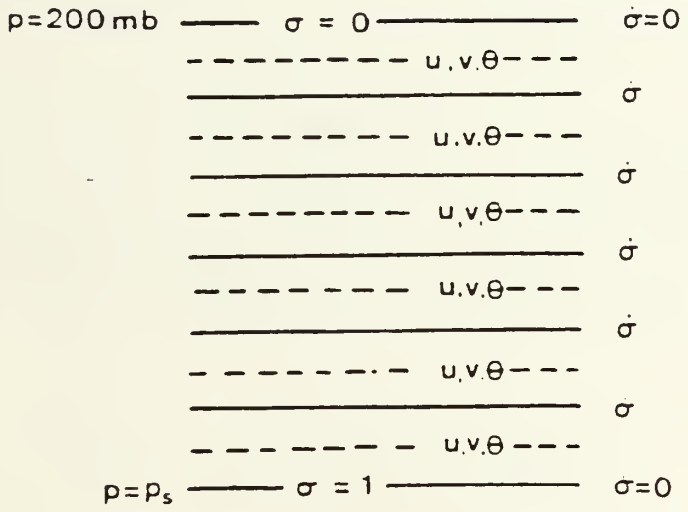

Figure 2.2. Vertical distribution of variables in a six-layer sigma coordinate system. Solid lines are σ-levels; dashed lines represent the middle of the layer (Arakawa and Lamb, 1977).

on the lower boundary, $\sigma = 1$. The vertical velocity, $\dot{\sigma}$, vanishes at the upper and lower boundaries and is diagnostically

derived on sigma levels. Wind (u,v) and potential temperature (θ) are computed at mid-layer.

C. FINITE DIFFERENCING SCHEMES

The model uses two time differencing methods--an Euler-backward scheme and the centered time differencing (or leapfrog) scheme. The model integration proceeds in a series of one Eurler-backward time step followed by four centered time steps. The Euler-backward scheme eliminates the computational mode of the centered scheme and selectively damps high frequency waves. The time step for these model integrations is 360 s.

III. MODEL INITIALIZATION

An analytical initialization scheme developed by Hayes (1985) is used. In this scheme, the initial mean wind is specified analytically using the Bickley jet described by Haltiner and Williams (1980). The initial surface pressure is derived from the wind using the geostrophic wind equation, and the initial temperature is derived using the thermal wind equation. In this research, a stable planetary wave and a synoptic scale perturbation are superimposed on a horizontally and vertically varying mean current.

A. INITIALIZATION OF THE MEAN FLOW

A baroclinic jet is located at 45° N and has a maximum velocity of approximately 46 m/s at 200 mb. The initial mean surface flow is given by the following equations:

$$\bar{u}_s(\phi) = \bar{u}_m \operatorname{sech}^2(\gamma(\phi-\phi_0)) \tag{3.1}$$

$$\bar{v}_s(\phi) = 0 \, . \tag{3.2}$$

It has the same latitudinal variation as the jet with a maximum speed of 5 m/s at 45° N decreasing to zero at the poles. The v-component of the wind is initially set to zero. The mean upper-level wind is given by:

$$\bar{u}_u(\phi, p(\sigma,\phi)) = \bar{u}_m \operatorname{sech}^2(\gamma(\phi-\phi_0))\left(\frac{\ell n(p_s/p)}{\ell n(p_s/p_m)}\right) \tag{3.3}$$

$$\bar{v}_u(\phi, p(\sigma,\phi)) = 0 \tag{3.4}$$

The wind varies in the vertical as the natural logarithm of pressure.

The mean surface pressure is calculated by integrating the geostrophic wind equation:

$$\bar{p}_s(\phi) = \exp\left[\ell n\, \bar{p}_s(\phi_0) - (a/R) \int_{\phi_0}^{\phi} f u_s(\phi)/\bar{T}_s(\phi)\, d\phi\right] \tag{3.5}$$

where $\bar{p}_s$ (ϕ_0 = 45° N) = 1013.25 mb and $\bar{T}_s(\phi)$ represents the mean surface temperature. Because the latitude structure of $\bar{T}_s(\phi)$ is unknown, $\bar{p}_s(\phi)$ is computed iteratively until the adjustment of $\bar{T}_s$ to the NACA standard for that $\bar{p}_s$ is less than 0.01° K.

The mean surface temperature is calculated by integrating the geostrophic thermal wind equation which gives:

$$\bar{T}(p,\phi) = \bar{T}(p,\phi_0) - \frac{\bar{u}_m\, a\, 2\, \Omega}{R\, \ell n\,(p/p_m)} \int_{\phi_0}^{\phi} \sin\phi \operatorname{sech}^2(\phi-\phi_0)\, d\phi \tag{3.6}$$

The integrals are computed using the Simpson Rule approximation. $T(p,\phi_0)$ is obtained from the NACA standard atmosphere:

$$\bar{T}(p,\phi_0) = \bar{T}(p_0,\phi_0) - \Gamma Z \tag{3.7}$$

where:

$$Z = \frac{T_0}{\Gamma}\left(1 - \left(\frac{p}{p_0}\right)^{\Gamma R/g}\right)$$

The value of T_0, 288° K, is taken from the NACA standard atmosphere using a standard surface pressure of 1013.25 mb. (Constants are defined in Appendix B.)

B. INITIALIZATION OF THE HAURWITZ WAVE

The initialization of the Haurwitz wave is accomplished in a subroutine developed by Dr. T. Rosmond.[1] The analytical solution for a Rossby wave on the surface of a sphere is described by Haurwitz (1940).

The Haurwitz wave has a zonal wave number 4 (Figure 3.1). The maximum meridional velocity is 16 m/s. The u and v components are given by the following equations:

$$U' = \frac{\partial \psi}{a \partial \phi} \tag{3.8}$$

$$V' = \frac{\partial \psi}{a \cos \phi \partial \lambda} \tag{3.9}$$

The equations of motion are used to derive the perturbation pressure:

---

[1]Personal communication, present affiliation Naval Environmental Prediction Research Facility, Monterey, CA.

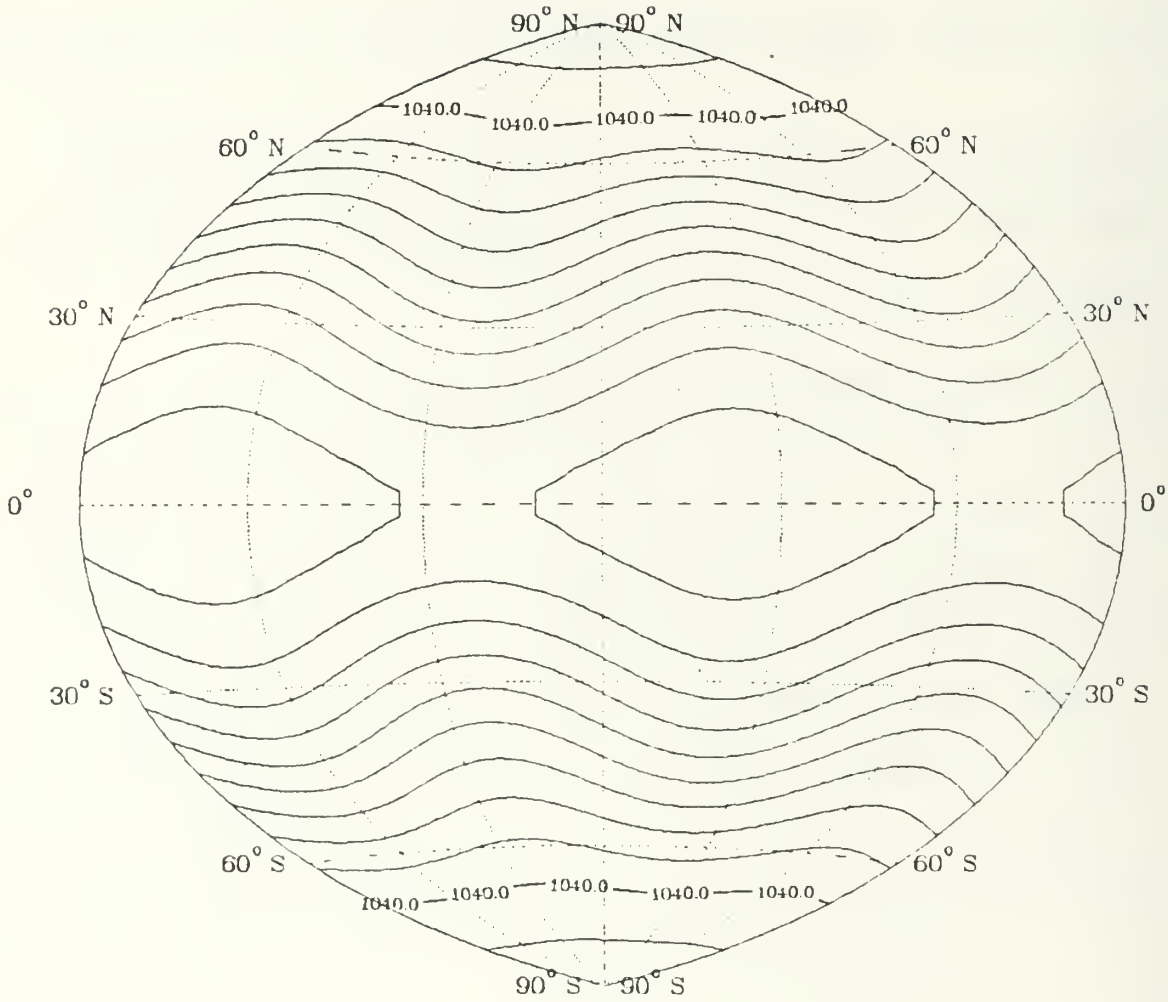

Figure 3.1. Sea-level pressure field for a stationary Haurwitz wave (3.10). Maximum meridional velocity is 16 m/s. Contour interval is 20 mb.

$$P' = C2(\omega+\Omega)\cos(\beta t+m\lambda)\left[\frac{n+1}{n}\sin\phi P_n^m - \frac{n-m+1}{n(n+1)} P_{n+1}^m\right] \qquad (3.10)$$

where $P_n^m(\sin\phi)$ is the associated Legendre polynomial and ω is the mean flow.

The equations listed above are for a Haurwitz wave superimposed on a mean flow. The Bickley jet and the Haurwitz wave schemes both have mean flow contributions, and one of the mean flows needs to be removed. Instead of using the formal analytical approach, the mean u, v and p for each J (latitude strip) is subtracted from the Haurwitz solution to provide the Haurwitz wave contribution. This method allows the sea-level pressures to be computed at the same time as the winds for the Haurwitz wave and the Bickley jet. Otherwise, the winds would have to be computed and then the pressures. The error in this approach should not have a significant effect on the results.

The Haurwitz wave u, v and p contributions are added to the Bickley jet and mean surface flow values. The surface values are spread to the upper levels using the equations described in the previous section.

C. THE PERTURBATION

The perturbation is a barotropic disturbance consisting of a longitudinal sine wave which is used for baroclinic instability studies. The maximum latitudinal amplitude in the meridional direction occurs at 45° N. The following equation describes the perturbation:

$$\Phi' = f_0(A \sin(m\lambda)\sin^{-2}(2\phi)) \tag{3.11}$$

The hydrostatic equation and the geostrophic wind equation are used to derive:

$$p' = -\frac{\bar{p}\Phi'}{RT} = -\frac{pf_0}{RT}(A \sin(m\lambda)\sin^2(2\phi)) \tag{3.12}$$

$$u' = -\frac{1}{af_0}\frac{\partial\Phi'}{\partial\phi} = -\frac{1}{a}(A \sin(m\lambda)2\sin(4\phi)) \tag{3.13}$$

$$v' = \frac{1}{af_0 \cos\phi}\frac{\partial\Phi'}{\partial\phi} = \frac{1}{a\cos\phi}(m\,A\cos(m\lambda)\sin^2(2\phi)) \tag{3.14}$$

where A = a·1 m/s. These perturbation quantities are added to the mean current and integrated forward in time to produce the forecast.

IV. ANALYSIS OF RESULTS

The hypothesis is that a cold surge results from the interaction of a growing wave number 8 cyclone moving eastward and a quasi-stationary stable forced wave number 4. Hayes (1985) showed that the basic baroclinic current, which is given in Equations (3.1) and (3.3), is unstable for wave number 8 but is stable for wave number 4. The stationary wave could be partially forced by the Himalayas. Three experiments were run to verify the hypothesis. Experiment I shows the effect of the stable wave number 4 on the southward migration of cold air. The effect of cyclogenesis in wave number 8 is depicted Experiment II. Experiment III is a combination of Experiments I and II.

A. EXPERIMENT I

In this experiment, the model is initialized with the stable wave number 4 and the baroclinic mean flow described in Chapter III.

The baroclinic jet is confined to the northern hemisphere to minimize forcing from the southern hemisphere. The model is integrated forward in time to 60 h. Sea-level pressure fields for 12, 24, 36, 48 and 60 h are shown in Figures 4.1 to 4.5. The potential temperature fields at σ = 11/12 for the same times are displayed in Figures 4.6 to 4.10. The corresponding wind vectors are shown in Figures

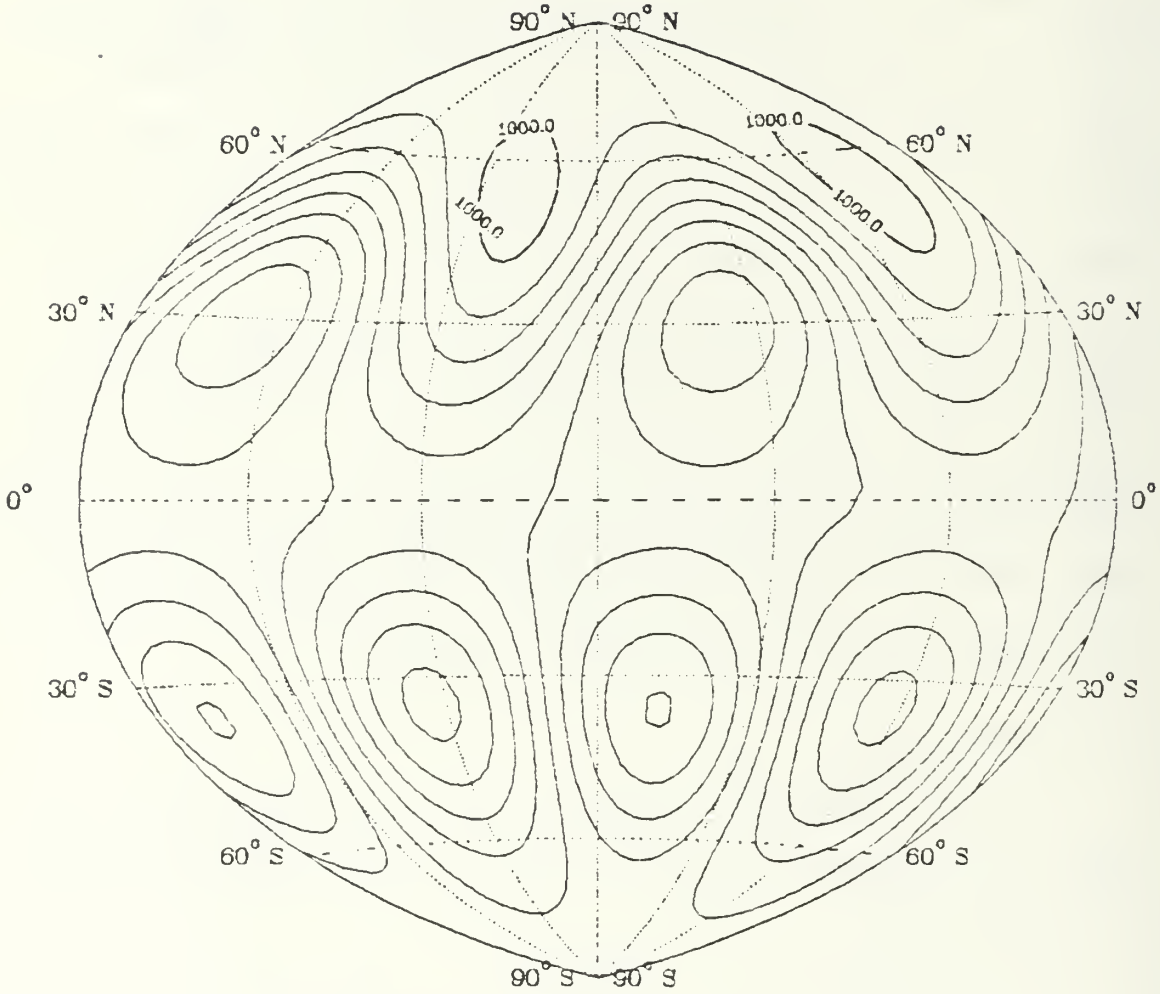

Figure 4.1. Sea-level pressure field at 12 h for Experiment I. Contour interval is 5 mb.

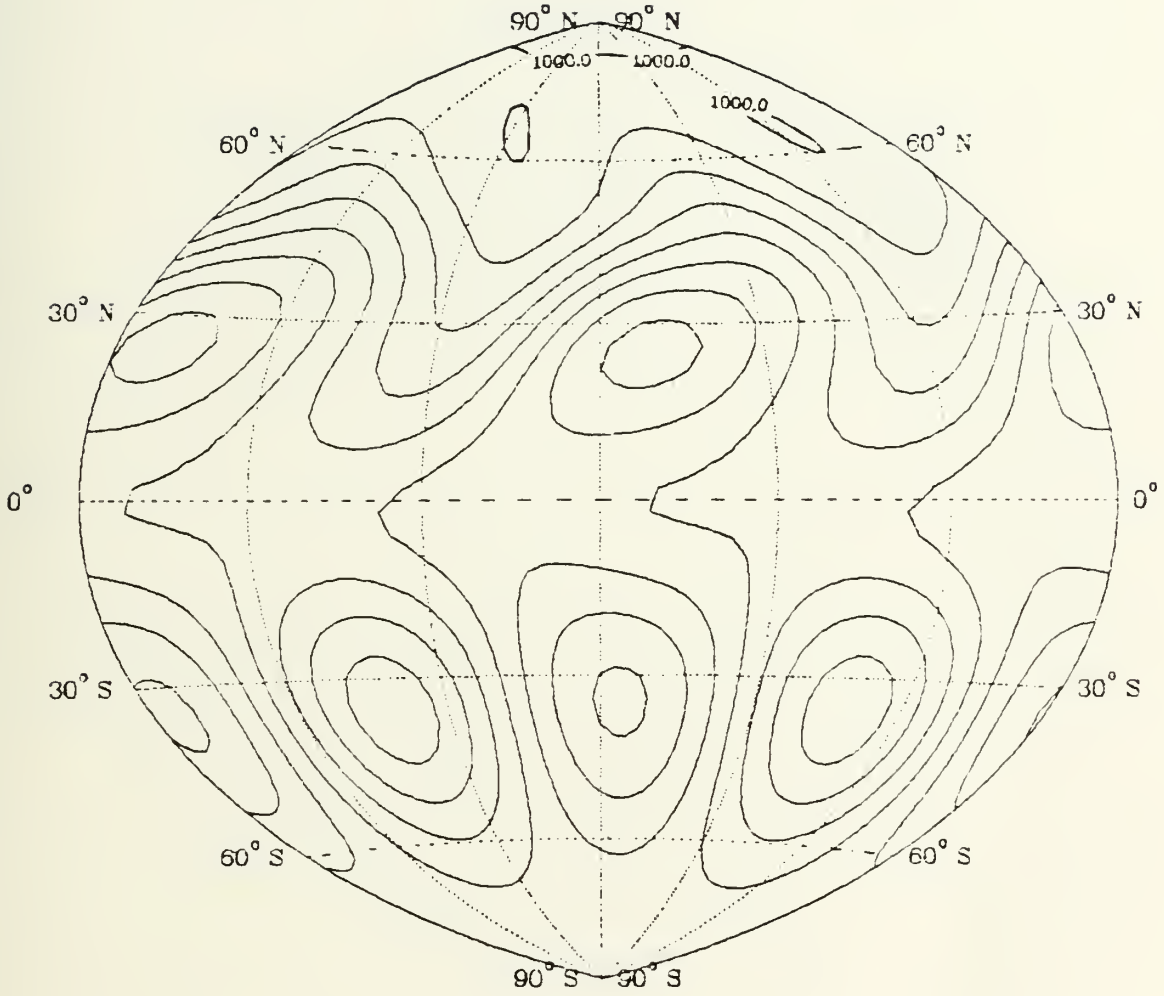

Figure 4.2. Sea-level pressure field at 24 h for Experiment I. Contour interval is 5 mb.

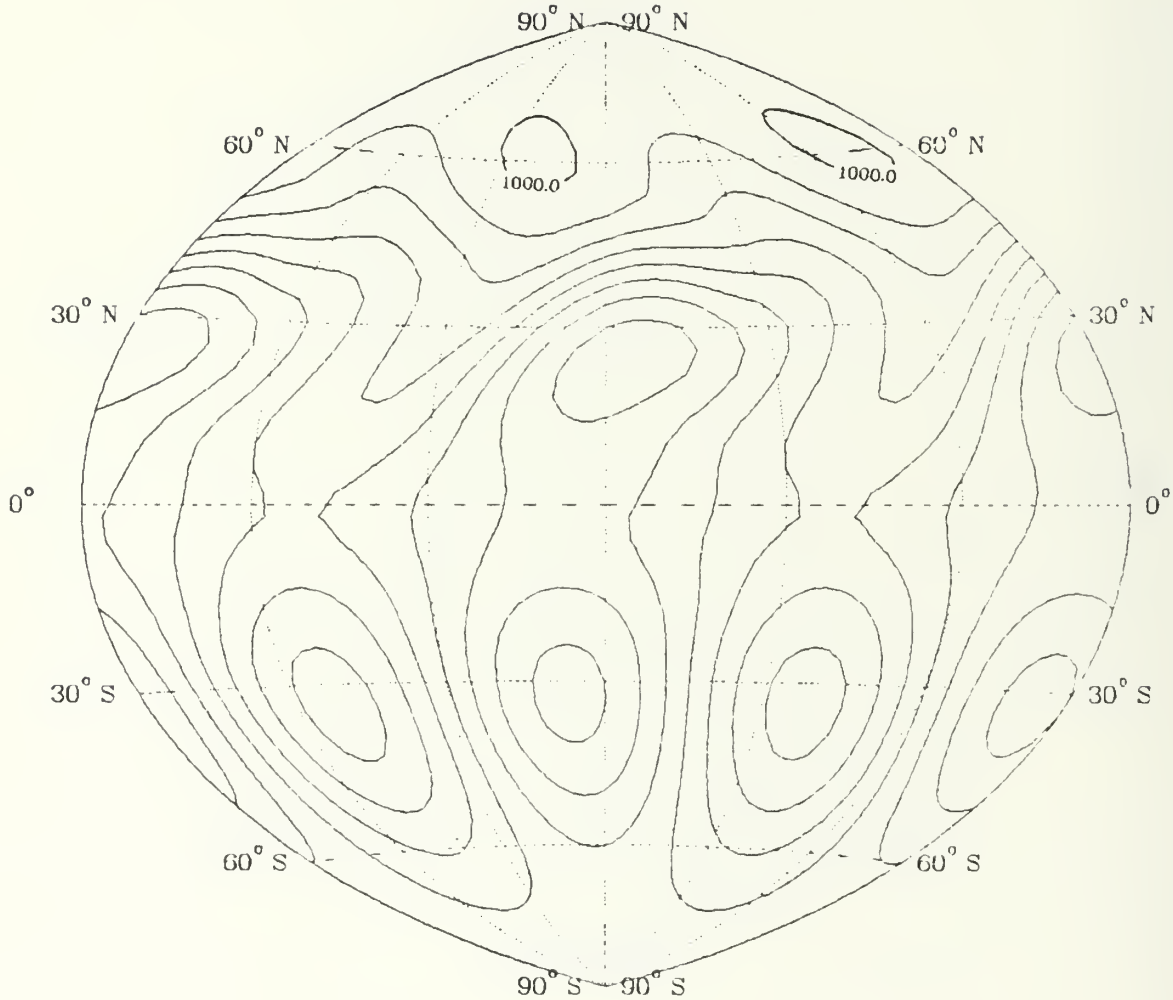

Figure 4.3. Sea-level pressure field at 36 h for Experiment I. Contour interval is 5 mb.

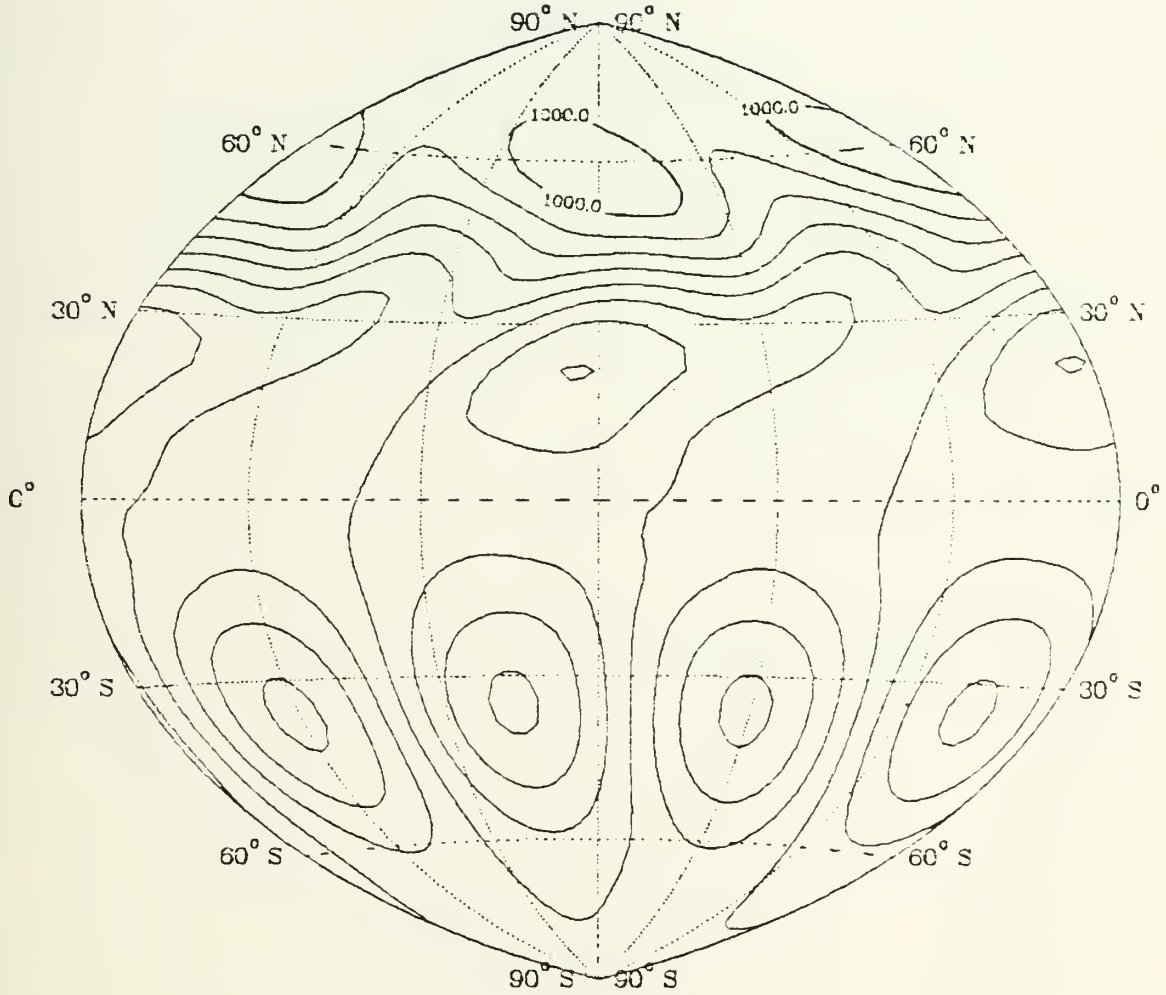

Figure 4.4. Sea-level pressure field at 48 h for Experiment I. Contour interval is 5 mb.

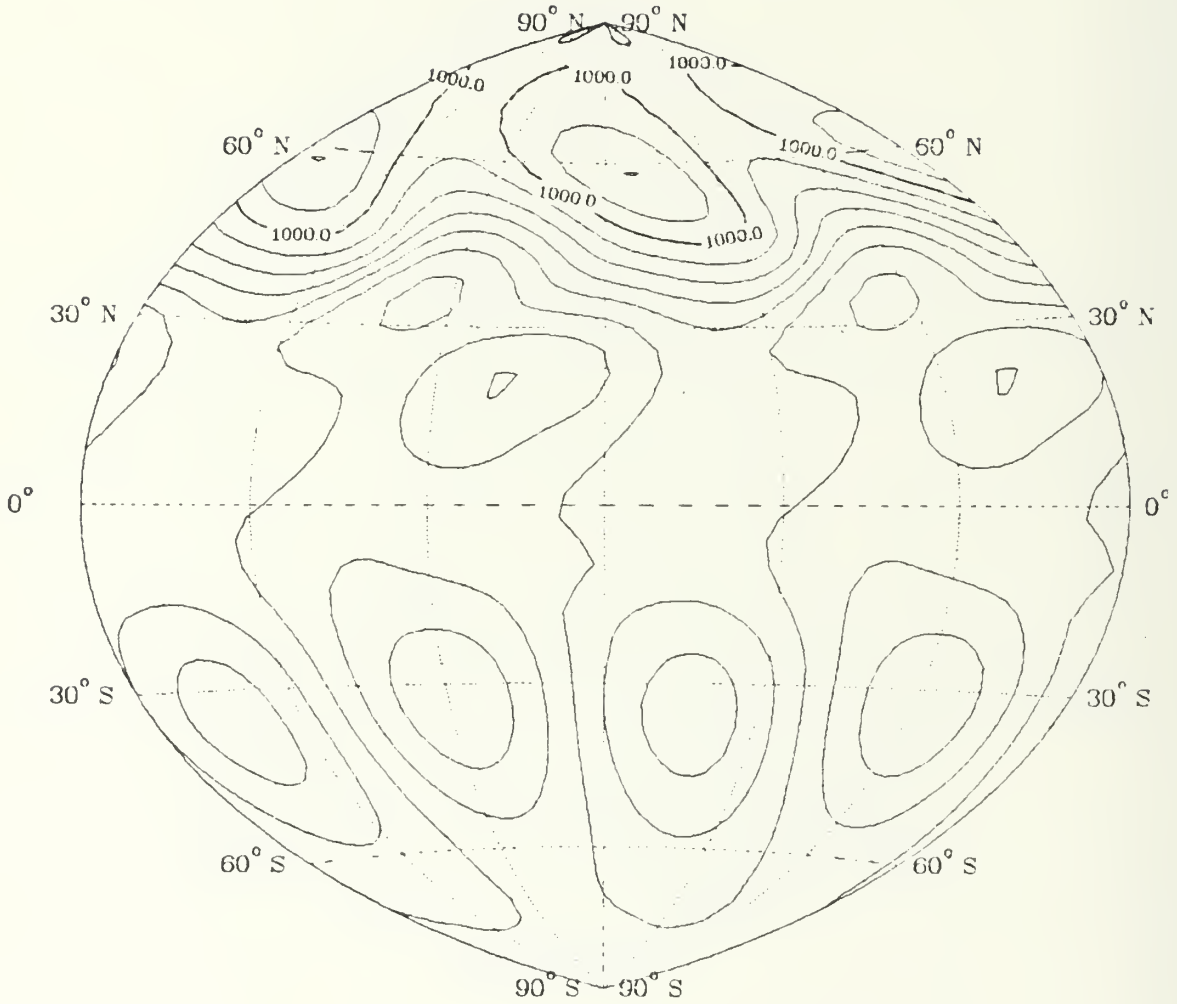

Figure 4.5. Sea-level pressure field at 60 h for Experiment I. Contour interval is 5 mb.

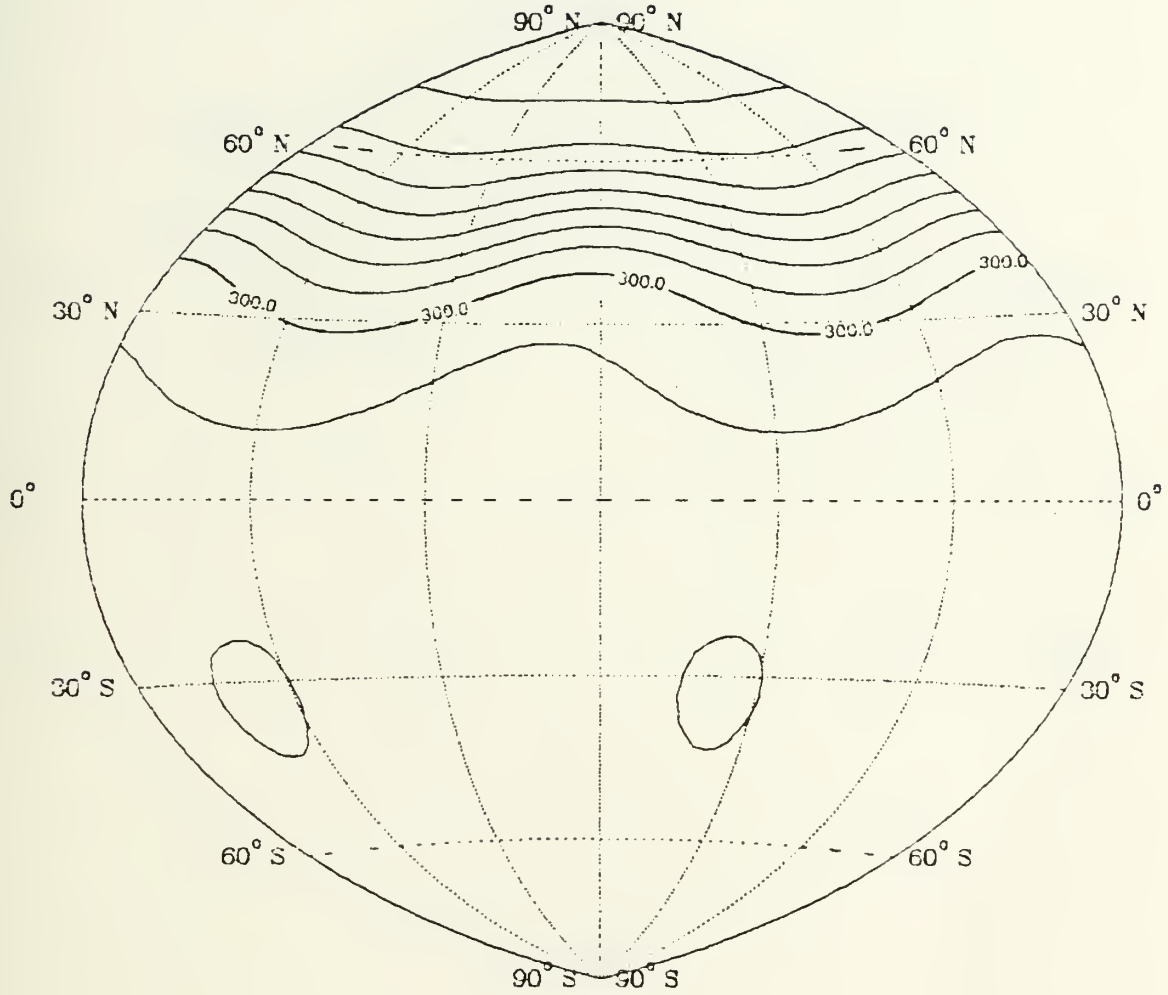

Figure 4.6. Potential temperature field at 12 h for Experiment I. Contour interval is 5° K.

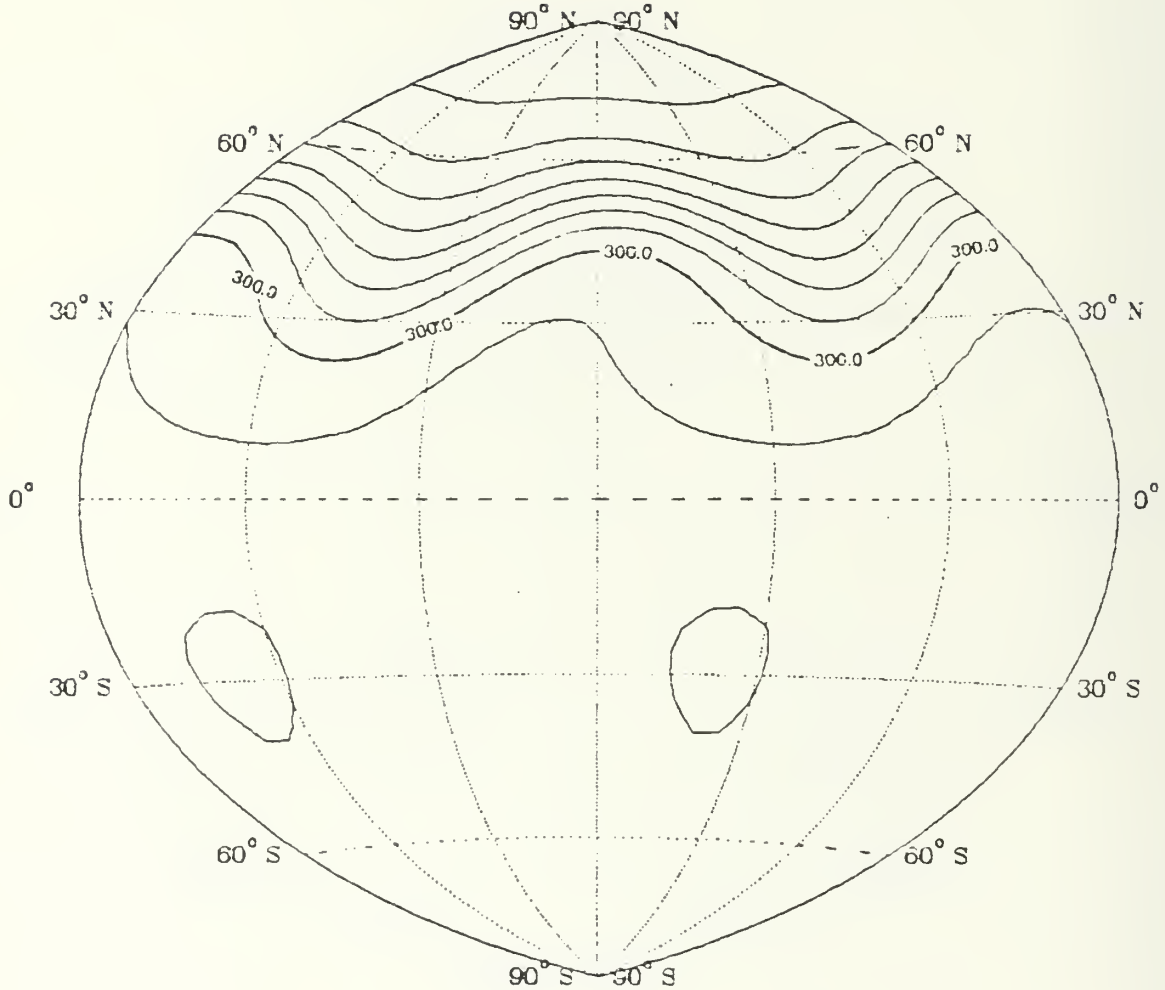

Figure 4.7. Potential temperature field at 24 h for Experiment I. Contour interval is 5° K.

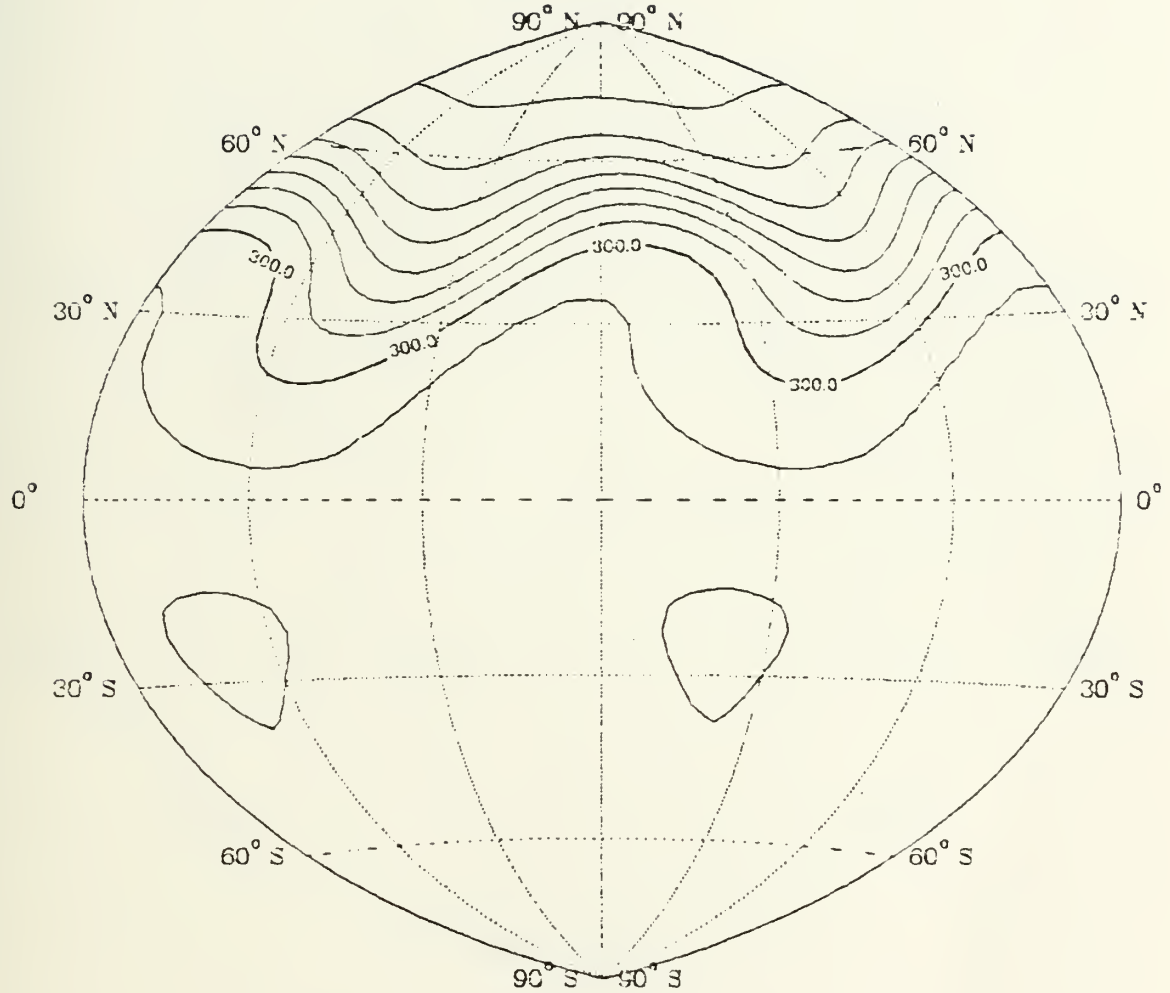

Figure 4.8. Potential temperature field at 36 h for Experiment I. Contour interval is 5° K.

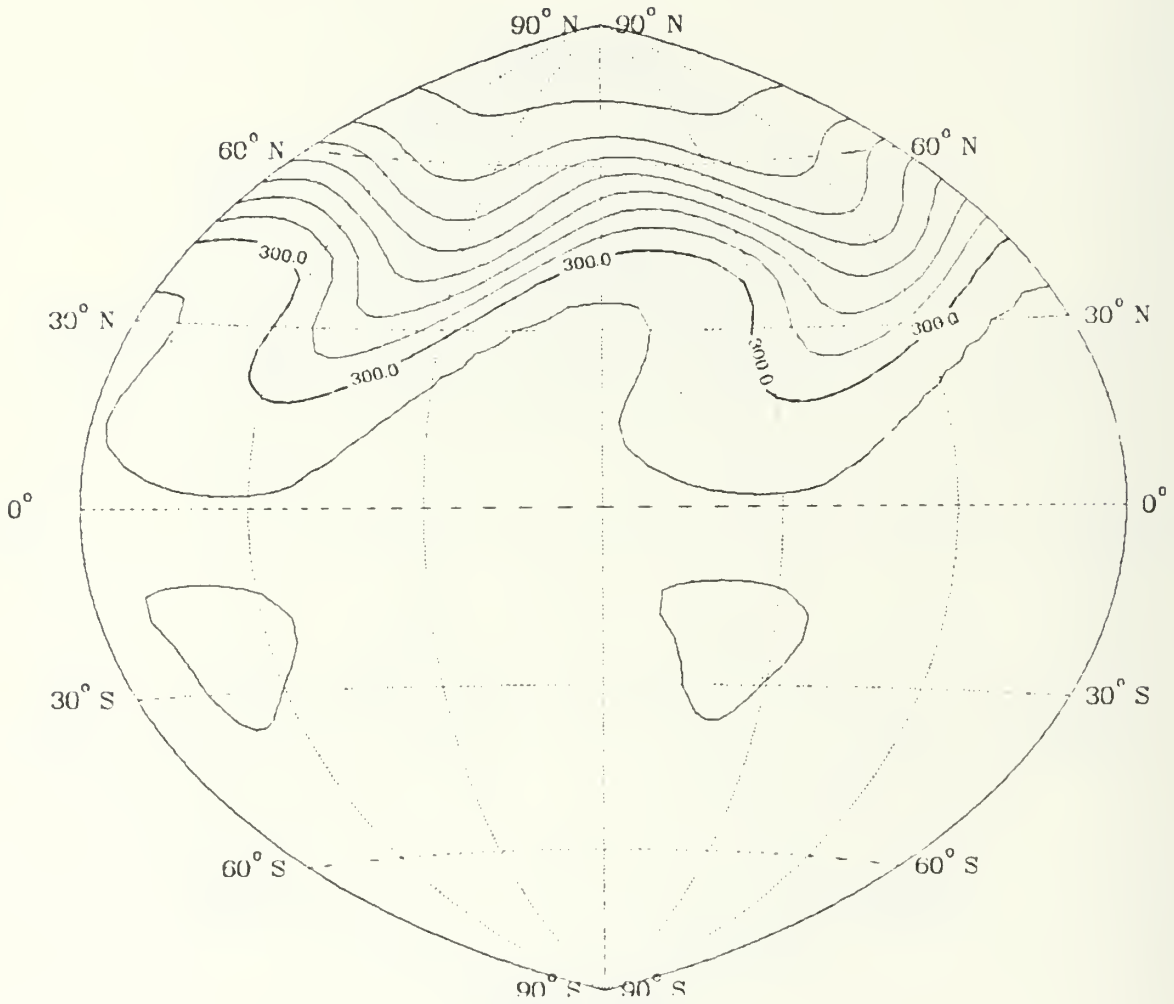

Figure 4.9. Potential temperature field at 48 h for Experiment I. Contour interval is 5° K.

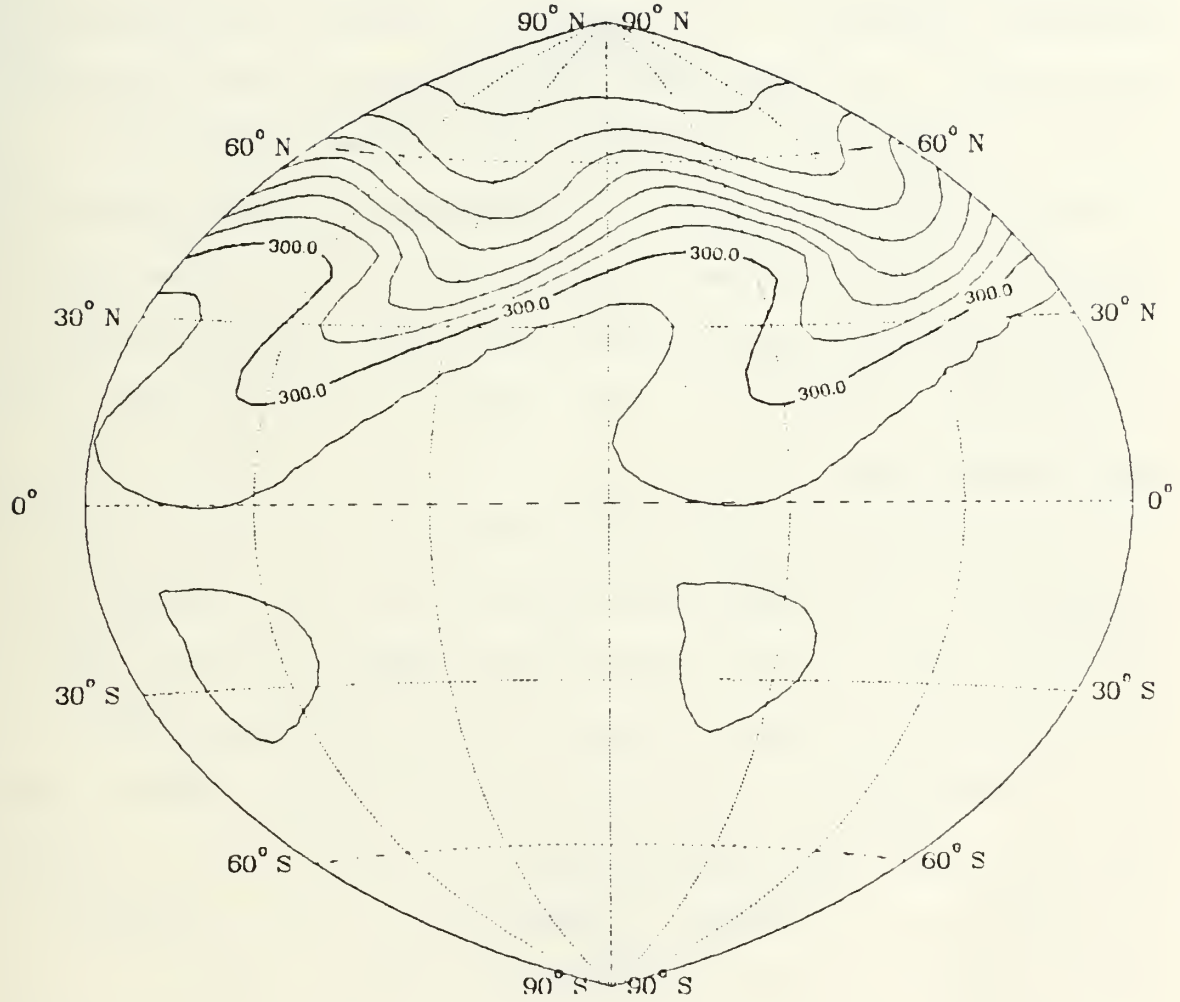

Figure 4.10. Potential temperature field at 60 h for Experiment I. Contour interval is 5° K.

4.11 to 4.15. The 90° sectors are plotted twice to produce hemispheric displays.

In the first twelve hours, the effects of the baroclinic jet on the wave are readily apparent (Figure 4.1). The wave has moved westward approximately 5° compared to 10° in the southern hemisphere. The westward movement is caused by the beta effect. A slight NE-SW tilt in the sea-level pressure field is apparent. The absence of a corresponding tilt in the southern hemisphere is consistent with the absence of the jet. In the northern hemisphere, the tilt is in the same sense as the shear on the south side of the jet indicating that the wave will lose energy to the mean flow. The wave should damp.

The pressure gradient has weakened as the cyclone and anticyclone are reduced in amplitude by 5 mb. However, at the same time, the amplitude of wave number 4 in the potential temperature field (Figure 4.6) has increased. The 305° K isotherm has moved south to near 10° N. The jet has advected that field eastward to a position 45° out of phase with the pressure field. Northeasterly winds of approximately 13 m/s are observed at 15° N (Figure 4.11).

By 24 h, the tilt in the sea-level pressure trough has increased to produce a stronger pressure gradient in the northwest quadrant and a weaker gradient in the northeast quadrant of the anticyclone. There has been a corresponding change in the wind field (Figure 4.12). A large area of

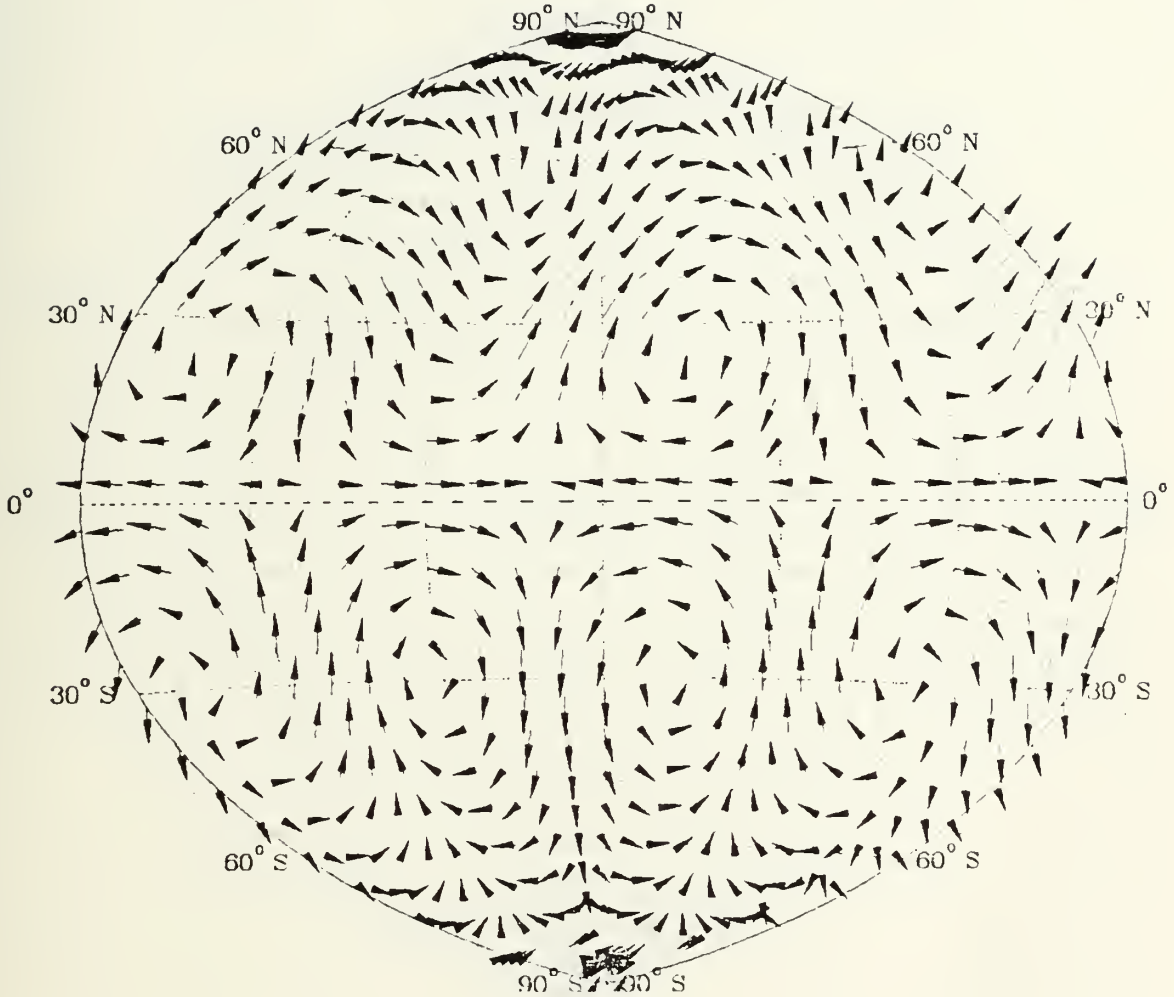

Figure 4.11. Wind vectors at 12 h for Experiment I. 8 mm = 20 m/s.

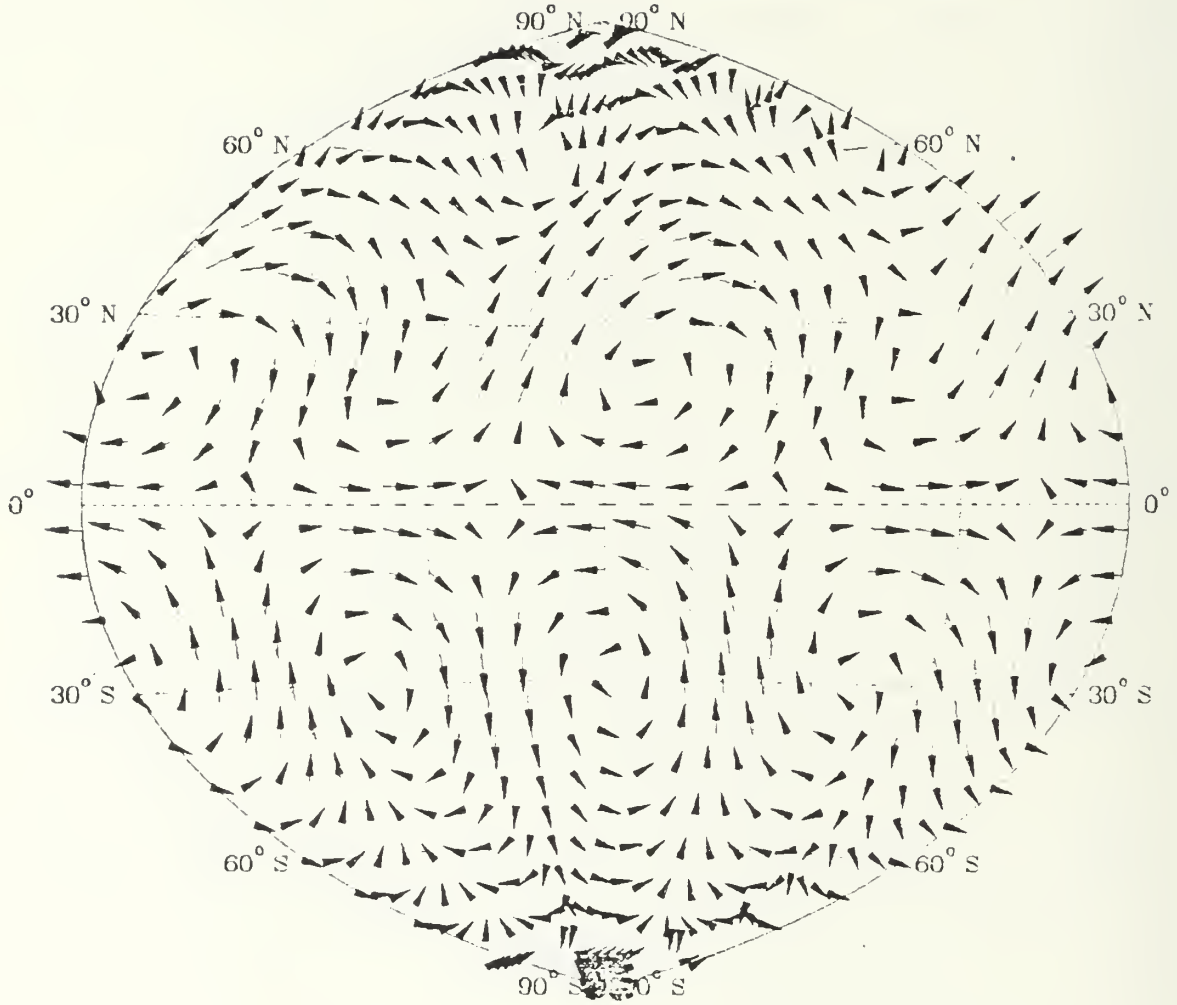

Figure 4.12. Wind vectors at 24 h for Experiment I. 7 mm = 20 m/s.

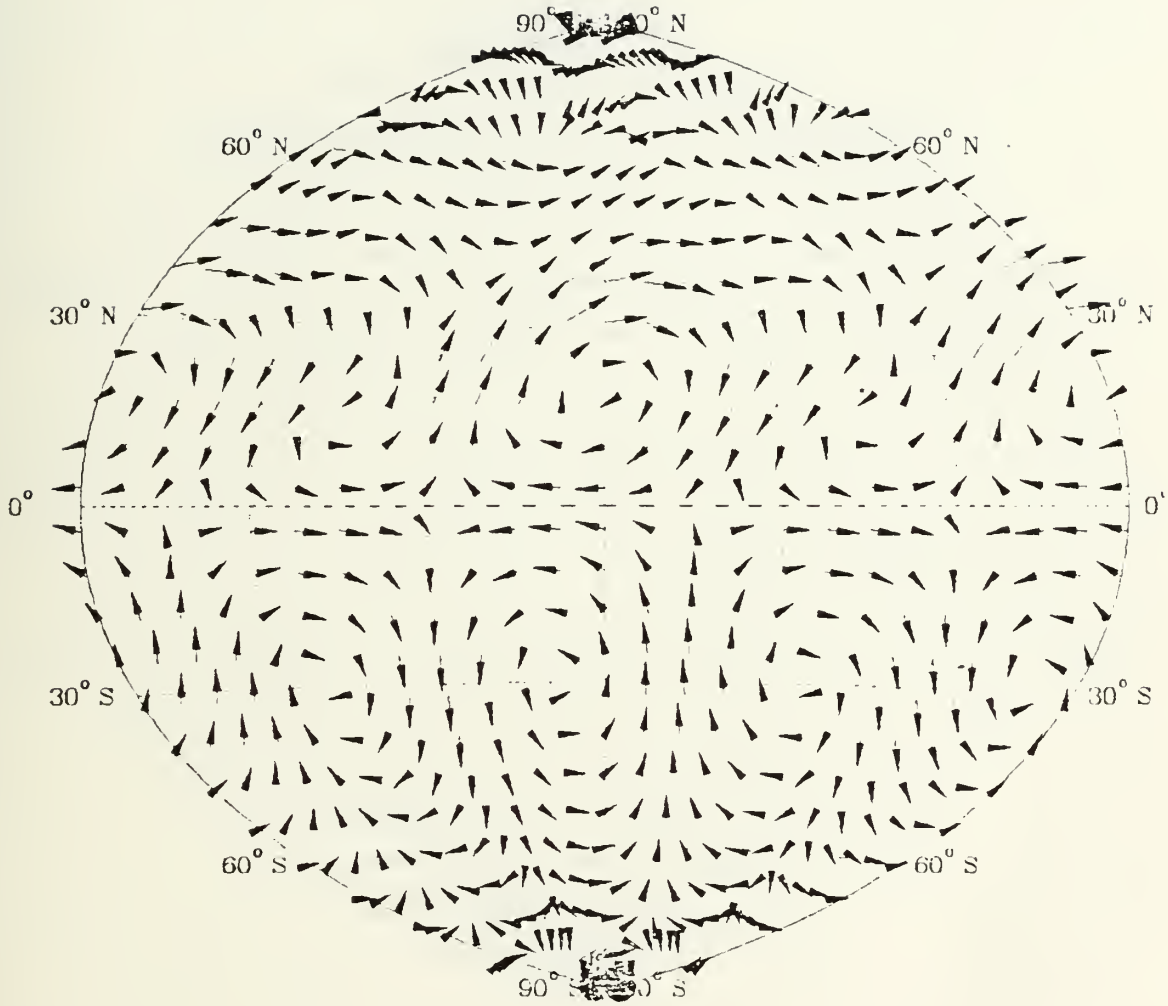

Figure 4.13. Wind vectors at 36 h for Experiment I. 7 mm = 20 m/s.

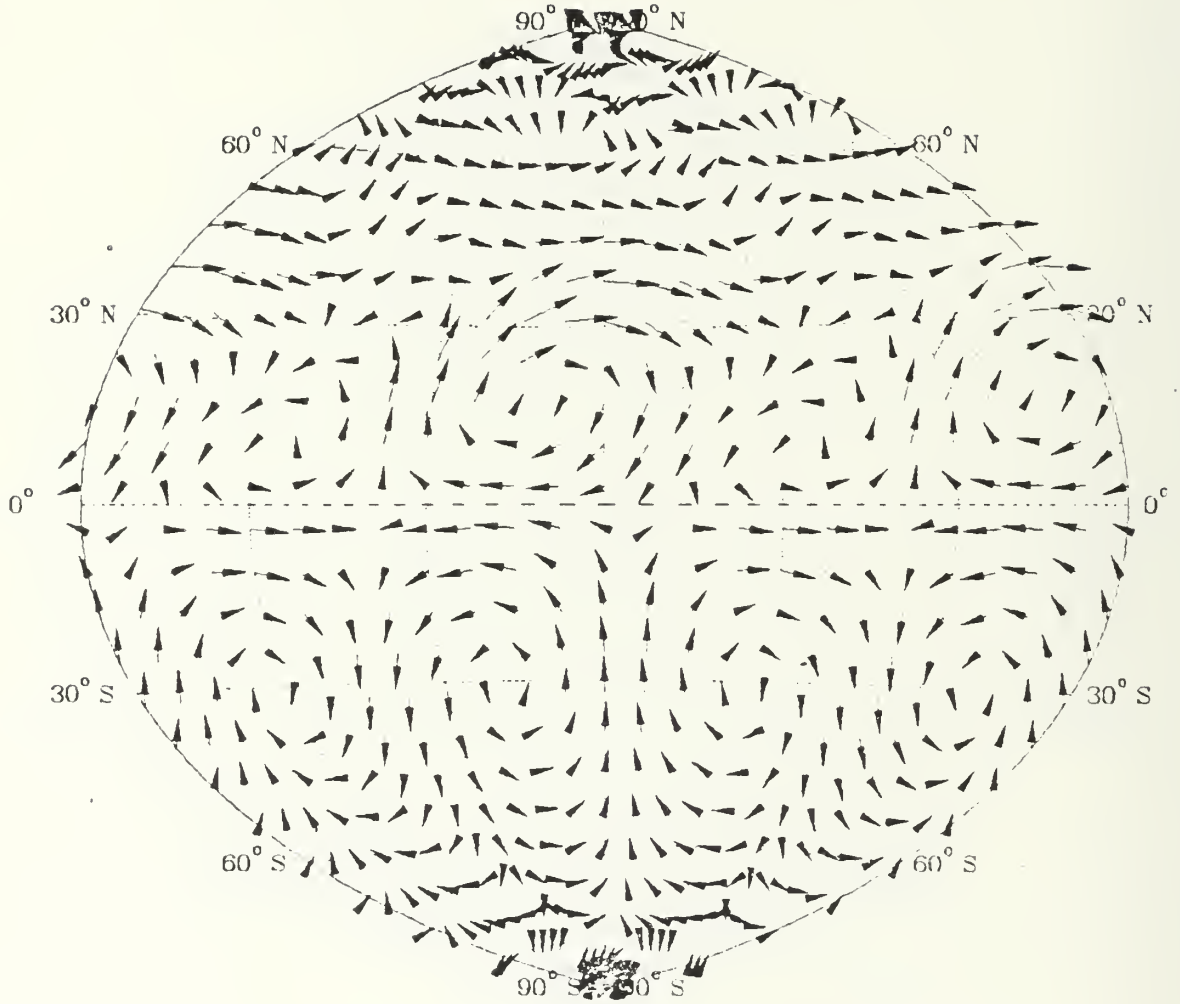

Figure 4.14. Wind vectors at 48 h for Experiment I. 8 mm = 20 m/s.

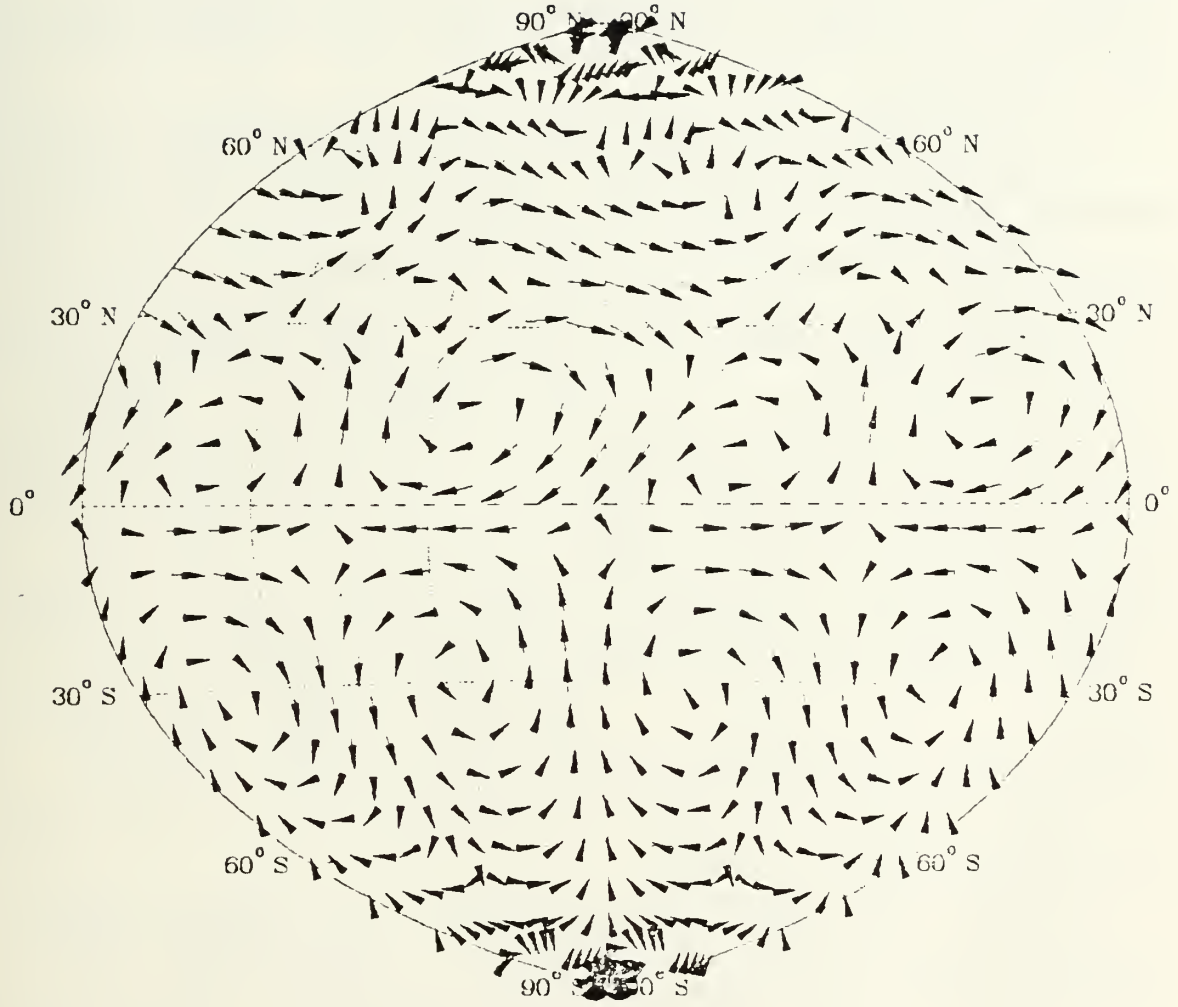

Figure 4.15. Wind vectors at 60 h for Experiment I. 7 mm = 20 m/s.

northeasterly winds is present in the southeast quadrant. Pressure centers have continued to weaken. A well-defined trough has formed along the equator with wind speeds as high as 13 m/s. The tilt and amplitude of the potential temperature wave have increased. Strong southwesterlies ahead of the trough are advecting warm air northward from 20° N to 45° N.

At 36 h, the anticyclone has intensified by about 5 mb. Ridging dominates the pattern particularly south of 30° N. The trough has filled as the flow has become more zonal. The cyclone has intensified slightly. Weak cyclonic flow is evident at the base of the trough (Figure 4.13). Amplification of the potential temperature field has continued with strong warm air advection ahead of the trough. Cold air advection behind the trough increased south of 20° N. With cold air moving south and warm air moving north, $\overline{V'\theta'}$ is positive, which indicates a baroclinic process. The area and speed of northeasterly winds on the eastern side of the anticyclone have increased.

At 48 h, the ridging south of 30° N has expanded eastward while the anticyclone weakened. North of 45° N the cyclone has intensified slightly and enlarged. The pressure gradient is oriented north-south. Although not evident on the pressure field, a weak cyclone has formed at the base of the trough (Figures 4.4 and 4.14). The wave structure in the potential temperature has amplified further. The 305° K

isotherm has moved to within 3° of the equator. North of 30° N, the field is 180° out of phase with that south of 30° N. Winds are northeasterly on the upwind side of the thermal trough.

In the next twelve hours, rapid development has occurred in the cyclone. The central pressure has dropped almost 10 mb. A secondary anticyclone formed 15° northwest of the primary high pressure center. The wave in the potential temperature field has continued to amplify. The 305° K isotherm has reached 1° S. The field does not reflect the surface pressure pattern north of 30° N. Northeasterly winds of greater than 15 m/s on the eastern side of the primary anticyclone are observed in the equatorial region (Figure 4.15). The secondary anticyclone is not adequately reflected in the wind fields indicating that this feature is not in geostrophic balance.

This experiment demonstrates the effects of a baroclinic jet on the stable wave number 4. The jet provided enough forcing to produce cold temperatures and strong northerly winds in the tropics. The 305° K isotherm moved southward from near 10° N to south of the equator. At 60 h, the secondary pressure centers indicate growth of wave number 8 which is unstable. This wave is induced by the nonlinear interaction of the long wave with itself.

B. EXPERIMENT II

In this experiment, the model was initialized with the baroclinically unstable mean flow and the wave number 8 disturbance described in Chapter III. The model was again integrated forward in time to 60 h. Sea-level pressure fields for 12, 24, 36 and 48 h are shown in Figures 4.16 through 4.19. The potential temperature fields for 12, 24, 36 and 48 h are depicted in Figures 4.20 through 4.23.

The results of this experiment are used to determine when to add the stable wave number 4 flow which will advect the synoptic scale disturbance southward in Experiment III. One requirement for this simulation is to have a sea-level pressure difference of at least 25 mb between high and low centers to ensure an adequate northwesterly current for surge initiation (Baker, 1983). Another requirement is the appearance of a high pressure center representing the Siberian anticyclone to the northwest of the low pressure center.

As shown in Figure 4.16, the disturbance is primarily a feature of the northern hemisphere mid- and upper-latitudes with a very flat pressure gradient in the tropical region. In the first twelve hours a low has formed in the trough approximately at 60° N. The trough has a slight NE-SW tilt and has moved eastward approximately 10° at 45° N. A sea-level pressure difference of greater than 25 mb exists between high and low centers. The potential temperature and

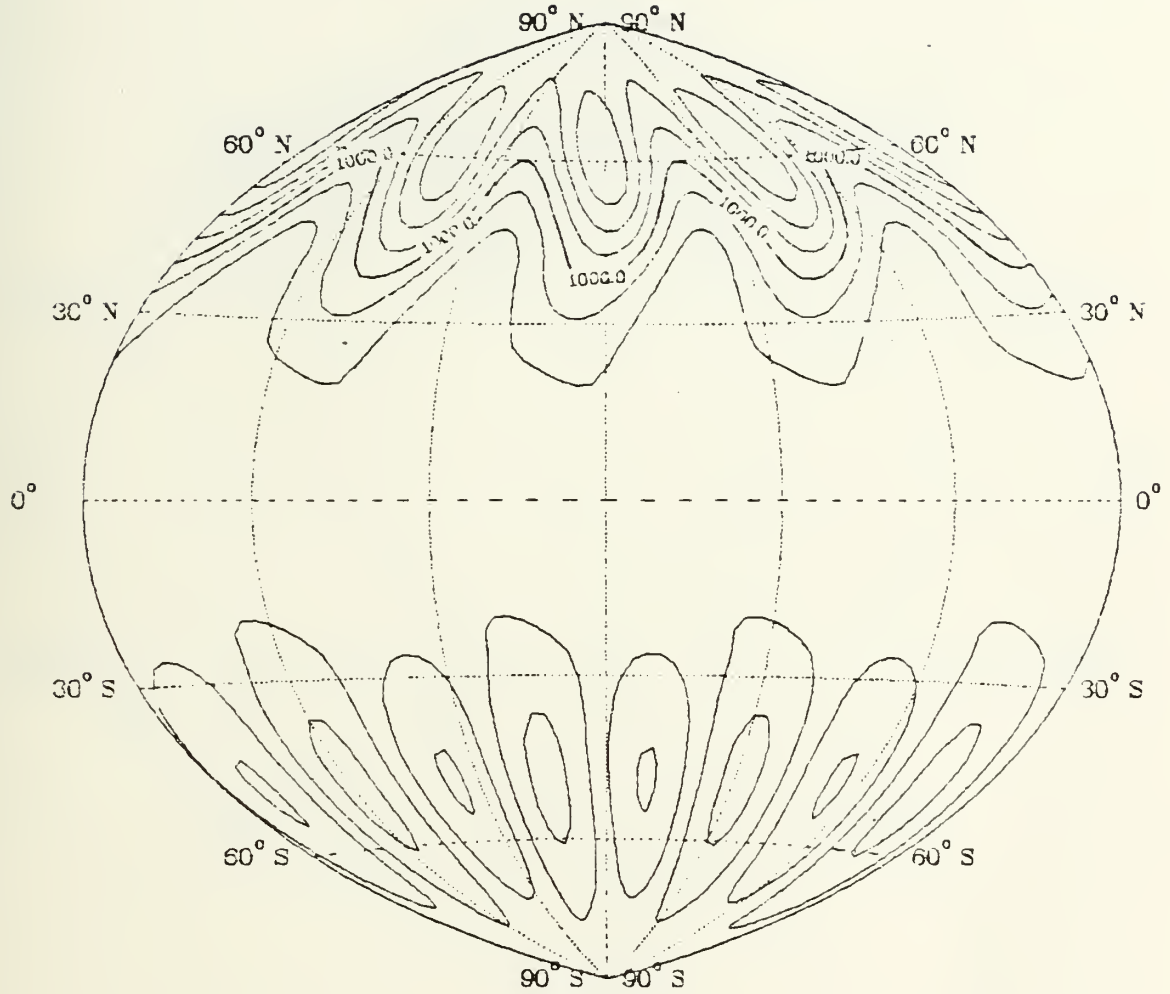

Figure 4.16. Sea-level pressure field at 12 h for Experiment II. Contour interval is 5 mb.

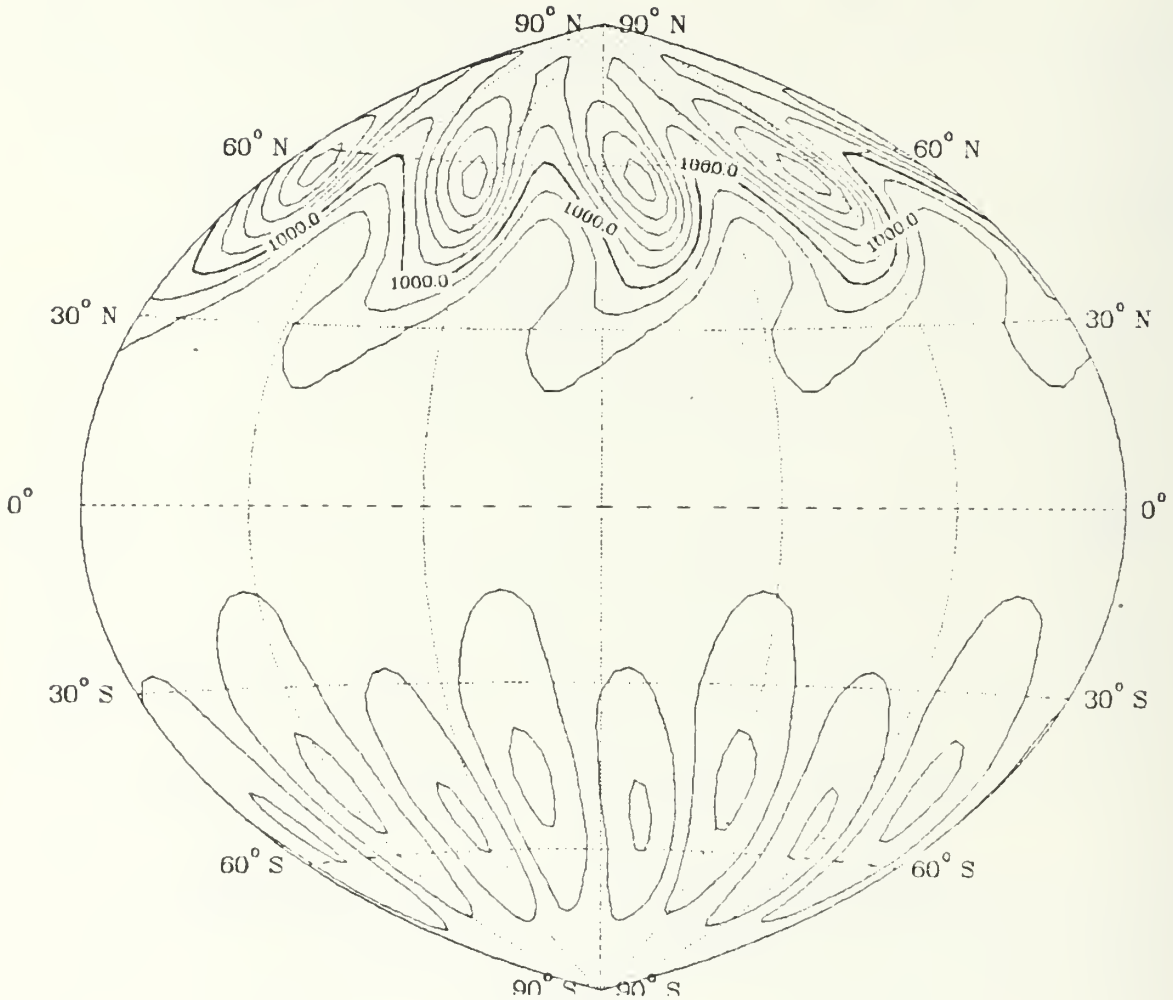

Figure 4.17. Sea-level pressure field at 24 h for Experiment II. Contour interval is 5 mb.

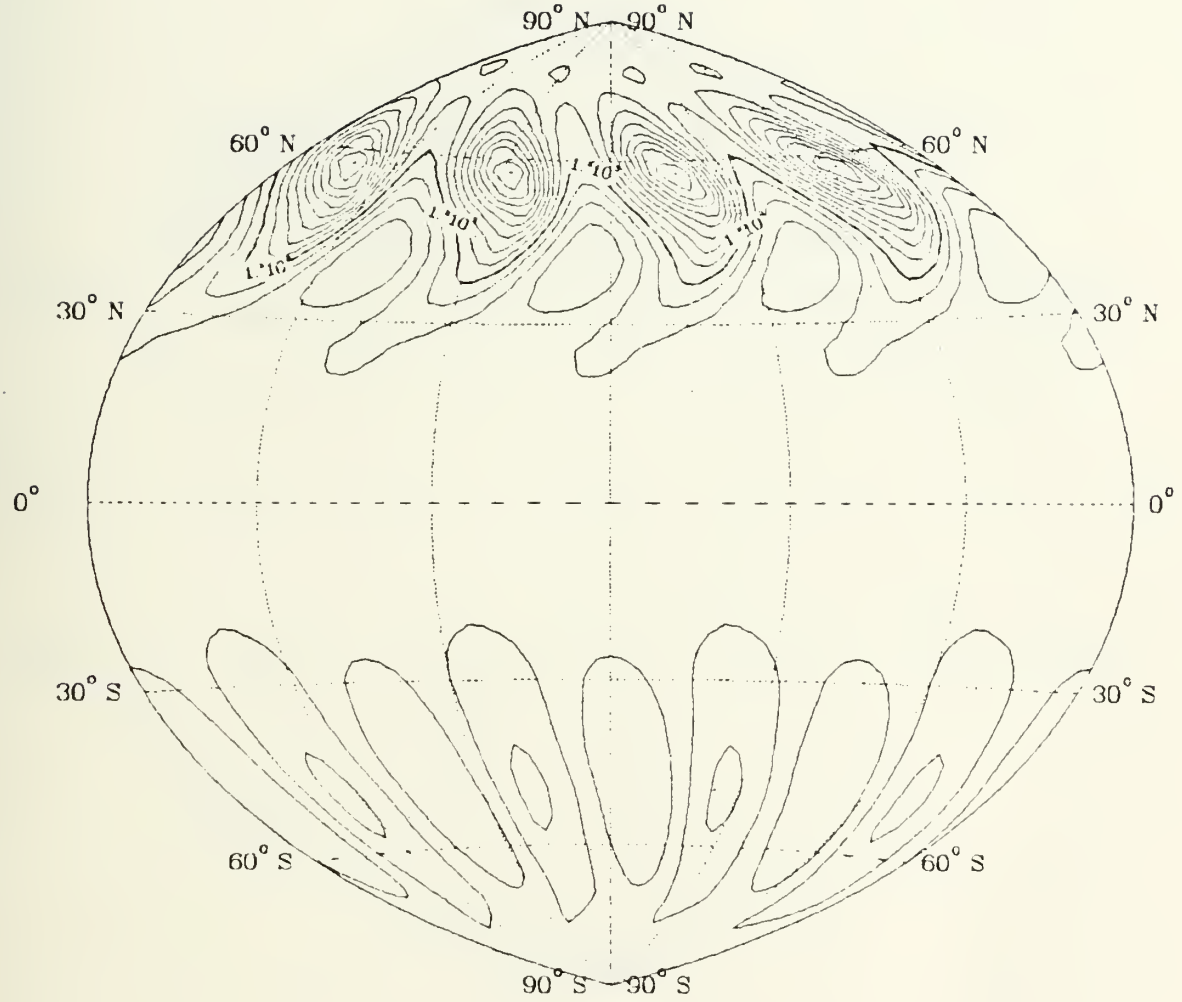

Figure 4.18. Sea-level pressure field at 36 h for Experiment II. Contour interval is 5 mb.

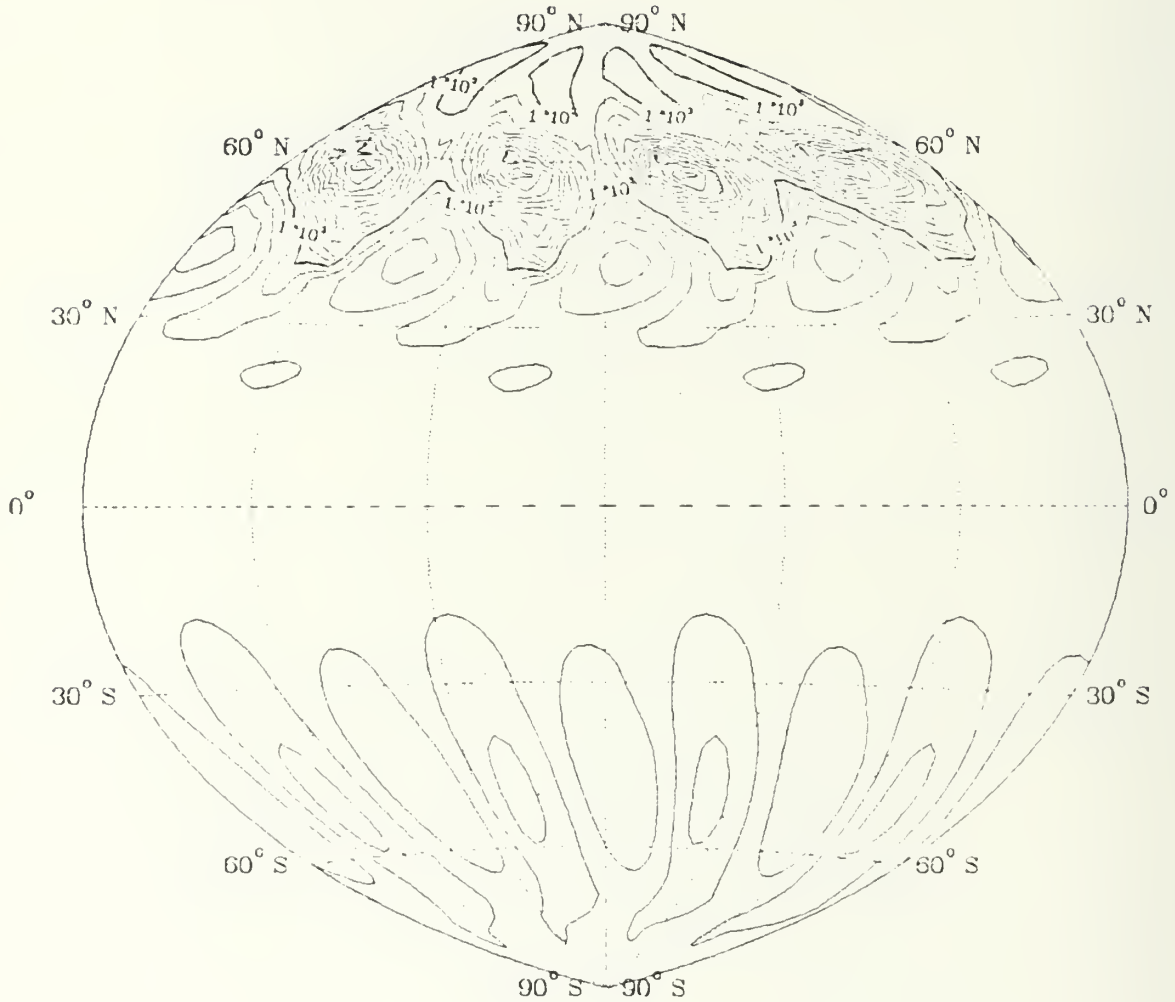

Figure 4.19. Sea-level pressure field at 48 h for Experiment II. Contour interval is 5 mb.

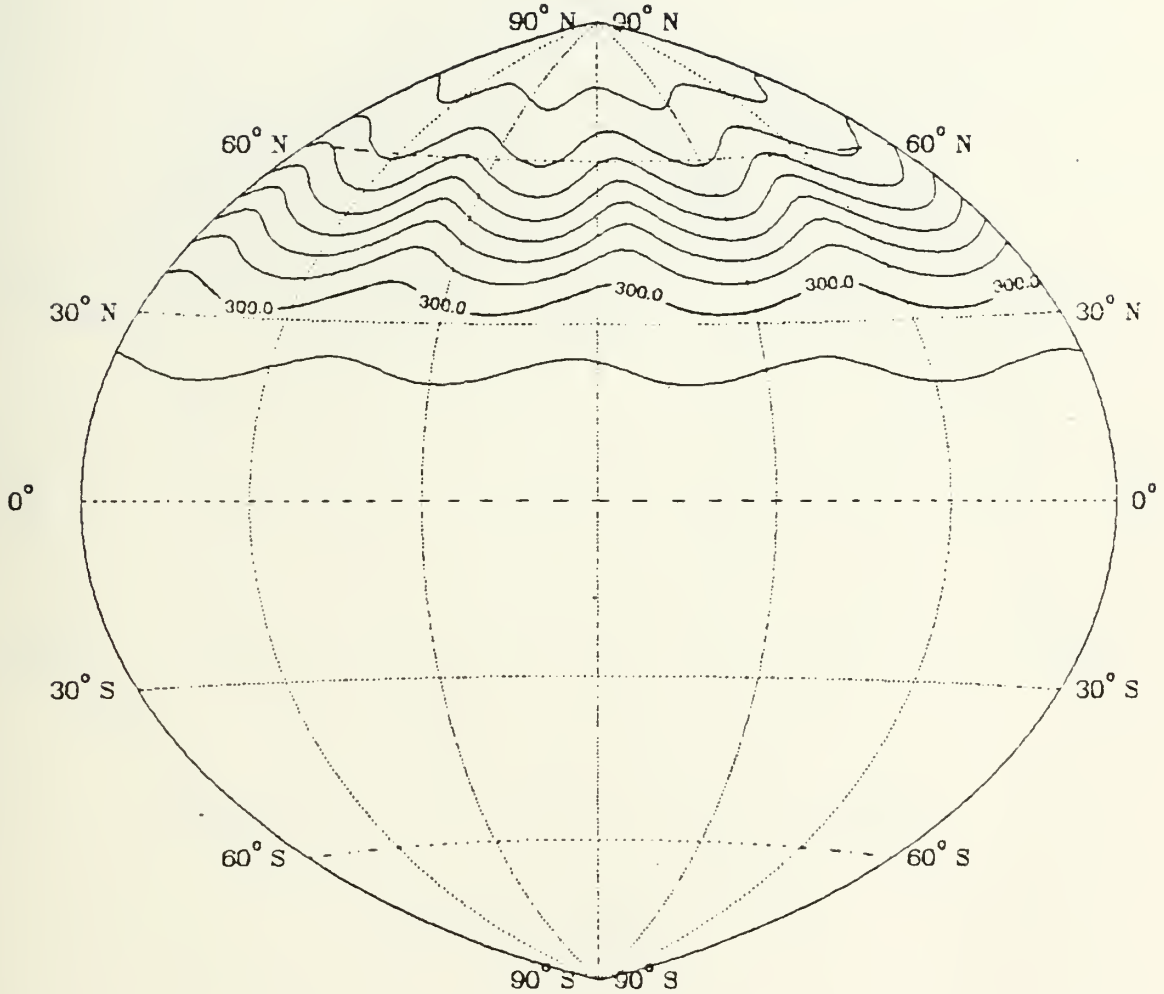

Figure 4.20. Potential temperature field at 12 h for Experiment II. Contour interval is 5° K.

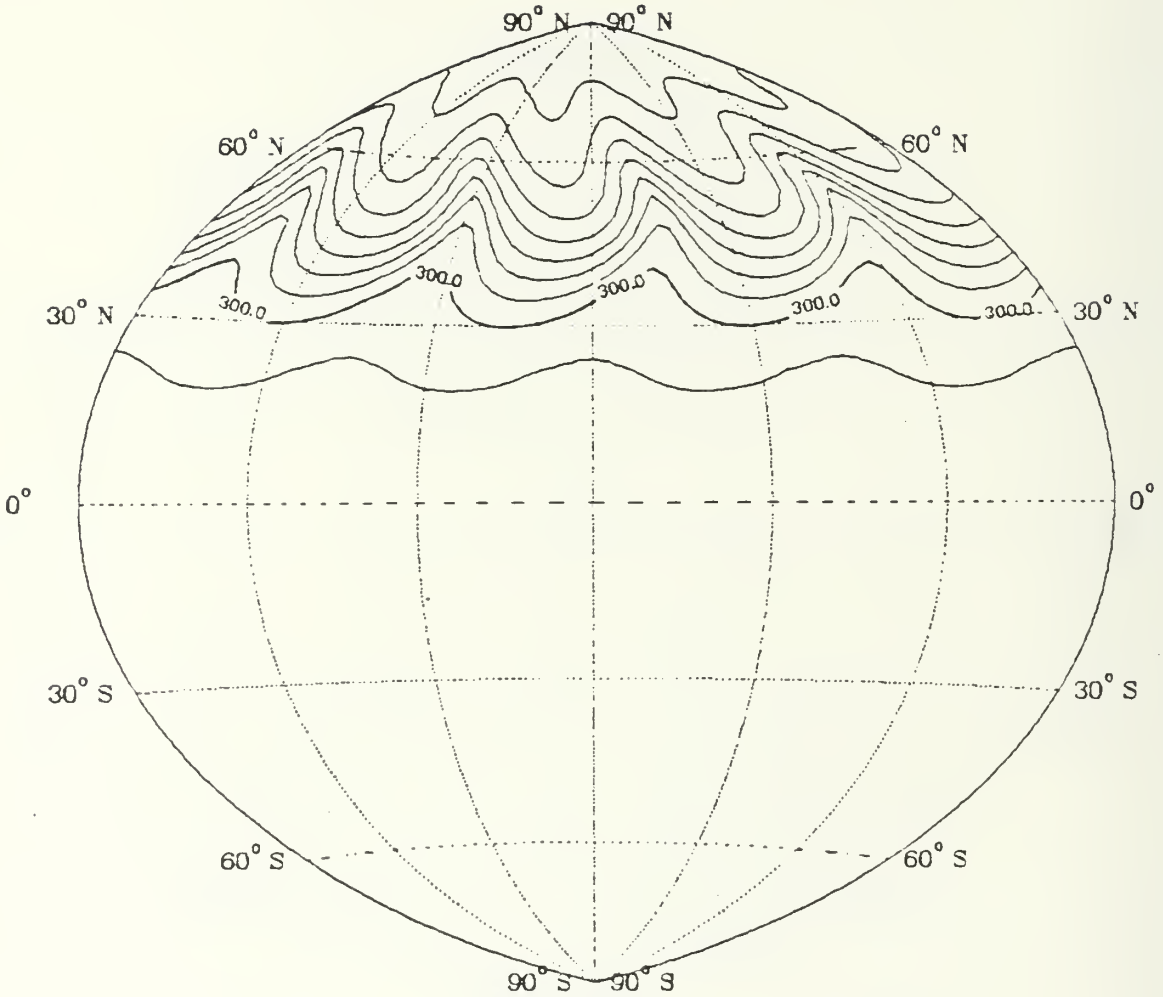

Figure 4.21. Potential temperature field at 24 h for Experiment II. Contour interval is 5° K.

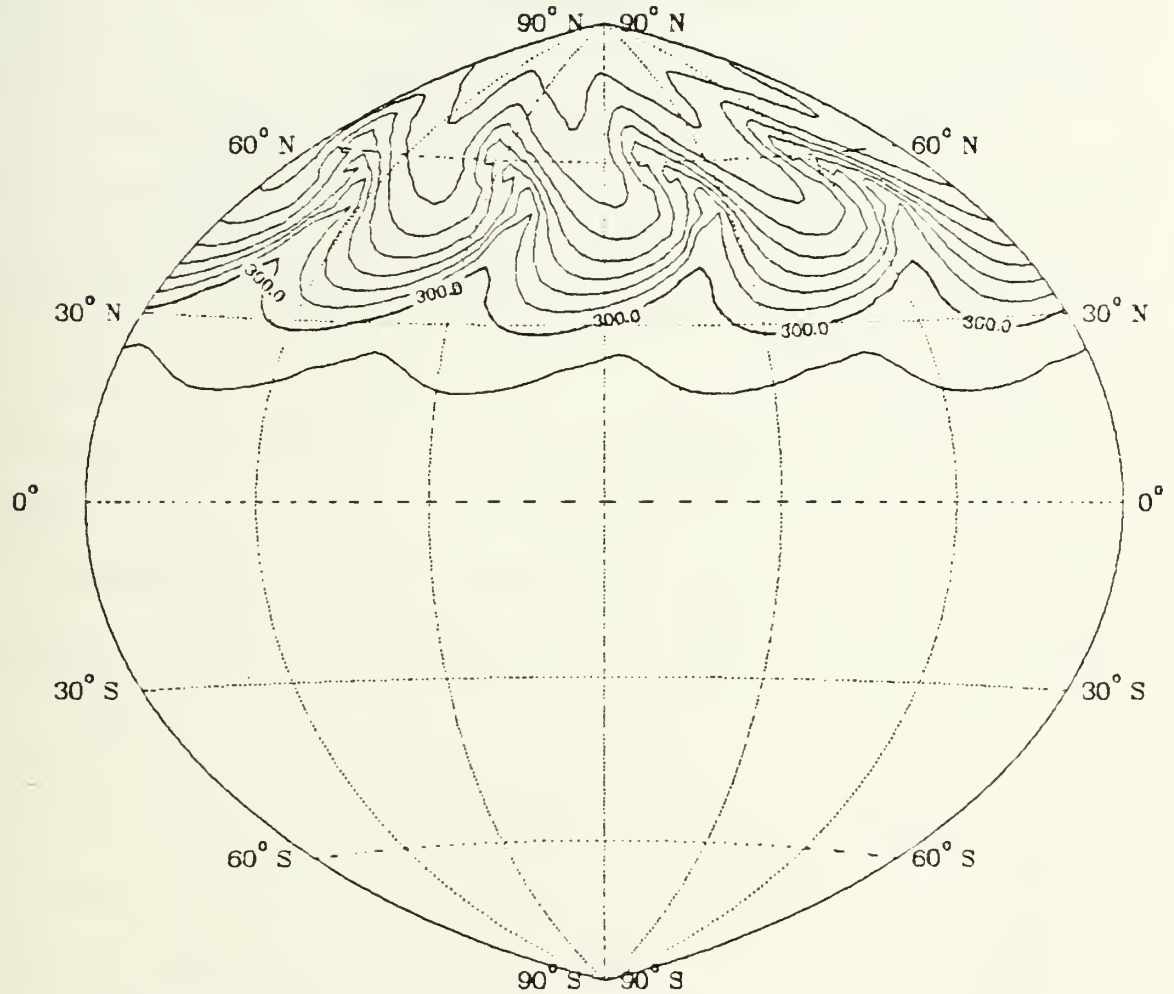

Figure 4.22. Potential temperature field at 36 h for Experiment II. Contour interval is 5° K.

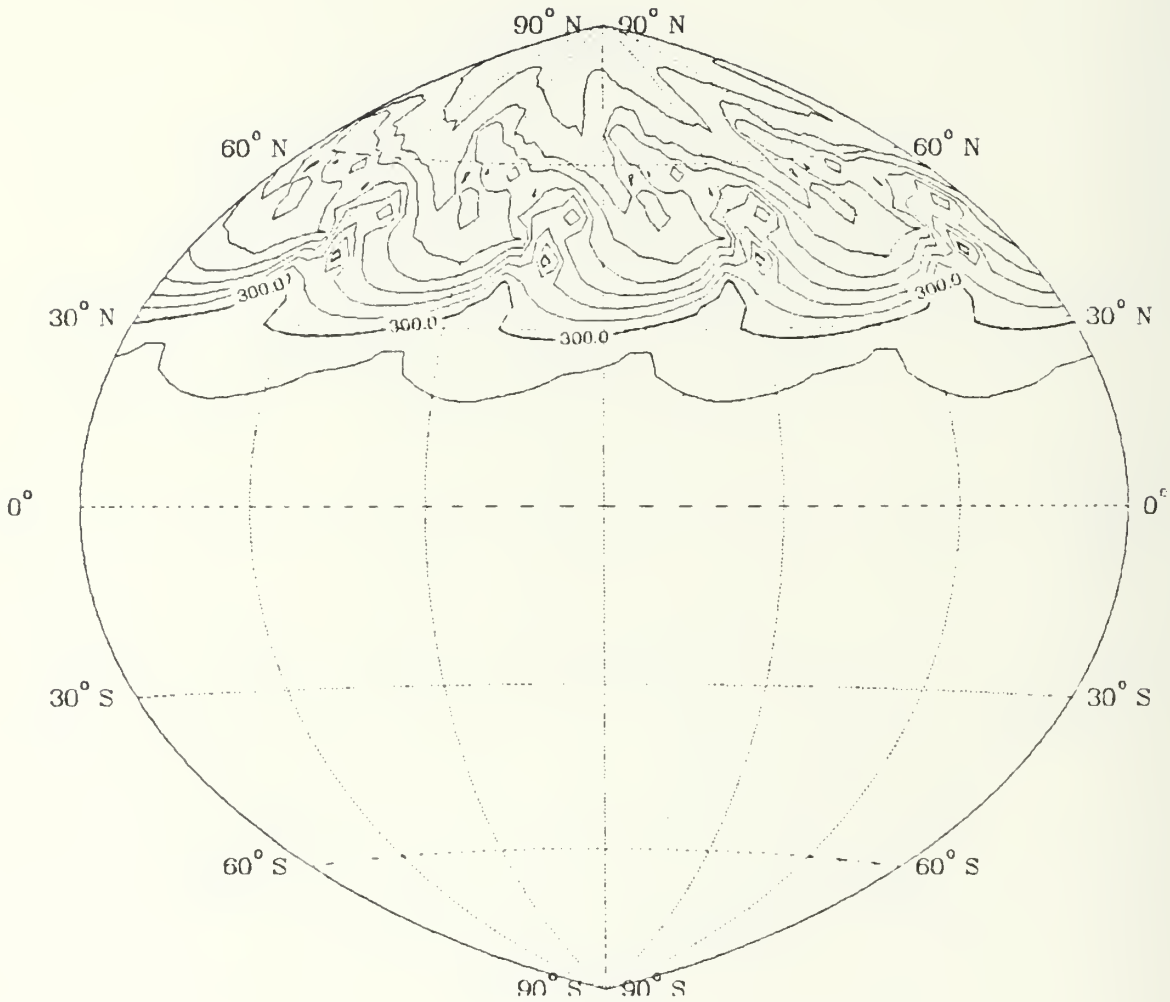

Figure 4.23. Potential temperature field at 48 h for Experiment II. Contour interval is 5° K.

wind fields indicate a baroclinic process with warm air being advected northward and cold air being advected southward.

At 24 h, the low centers have moved 5° southeast of their previous positions and have intensified. A sharp surface-pressure ridge extending north to 80° N separates the disturbances. Eastward movement of the trough has continued at the previous rate. Development of the primary disturbance in the wind and potential temperature fields parallels that of the pressure field. Some short wave noise is apparent in the wind field. Noise is to be expected because no surface frictional dissipation, diffusion or smoothing techniques are included in the model. These techniques tend to dissipate surge energy, and the objective of this study is the simulation of intense monsoon surges.

From 24 h to 36 h, rapid deepening has occurred in the cyclone. The central pressure of the low has dropped at least 15 mb. The ridge between low centers has weakened, but the sea-level pressure difference between high and low centers has increased to more than 50 mb. A broad band of low pressure appears to dominate the zone between 50° N and 60° N. Surface warm and cold fronts are clearly evident in the temperature field at 36 h (Figure 4.22). The potential temperature shows a poleward flux of warm air and a migration of cold air south of 30° N.

The rapid deepening of the surface pressure low continued between 36 h and 48 h. The central pressure dropped approximately 10 mb. High pressure centers formed near 40° N, and the sea-level pressure difference between the high and low pressure centers is greater than 70 mb. The northern portion of the strong baroclinic zone is advected southeastward about 7° latitude. The potential temperature field shows some additional migration of cold air south of 30° N (Figure 4.23) compared to 12 h earlier. At 60 h, the 300° K isotherm follows the 30° N latitude circle, and the 305° K isotherm is a little south of 20° N.

Analysis of these fields reveals several key features. A sea-level pressure difference of greater than 25 mb between high and low centers is present from 12 h onward. The sea-level pressure difference actually increases throughout the run. A high pressure center northwest of the low is best depicted at 24 h; it weakens afterwards. A strong Siberian high is not observed probably due to the presence of a strong jet and lack of topographic and radiative forcing. The period of most rapid cyclonic development is between 24 h and 36 h. The cold air and strong northerly winds never penetrate south of 30° N.

Based on these results, wave number 4 should be added to the growing cyclone between 24 h and 36 h. The most rapid cyclogenesis is occurring at this point. Adding the larger scale wave will further advect the cold air south to help initiate the surge.

C. EXPERIMENT III

The initialization for this experiment is the same analytic scheme as Experiment II. However, after 36 h of model time, the wave number 4 fields are added. (Note: The zonal mean has been removed from the wave number 4 fields.) Sea-level pressure, potential temperature, and wind fields are depicted in Figures 4.24 through 4.35.

The development of the disturbance through 36 h is described in Experiment II. The effect of wave number 4 on the disturbance is readily apparent when comparing the 36 h fields of Experiments II and III. A high pressure center of at least 1030 mb forms in the ridge. The primary cyclone deepens another 35 mb with the addition of wave number 4. This rapid deepening produces a pressure surge.

The second stage of the monsoon surge is characterized by a sharp drop in surface dewpoint (Baker, 1983). This model does not include moisture or its effects, but observational studies (Chang et al., 1979 and Chu, 1978) show that this stage can also be associated with a drop in surface temperature. At 36 h, a trough of cold air extends southward to approximately 17° N at the base of the high pressure, however, the potential temperature gradients are very weak south of 30° N. The winds are primarily northerly at 15 m/s on the eastern side of the anticyclone.

From 36 h to 48 h the weaker low moved east toward the stronger low. The long wave ridge weakened and tilted more

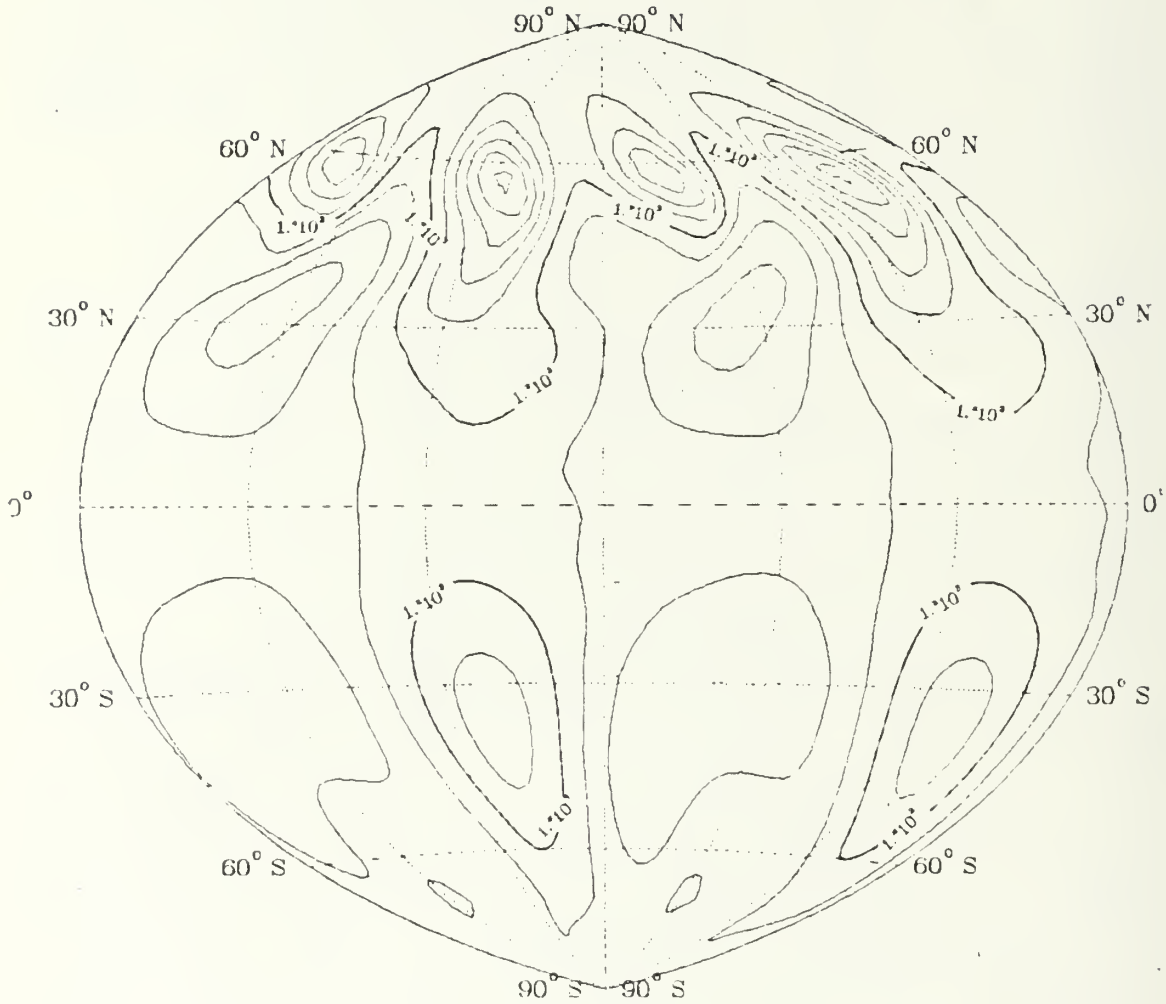

Figure 4.24. Sea-level pressure field at 36 h for Experiment III. Contour interval is 10 mb.

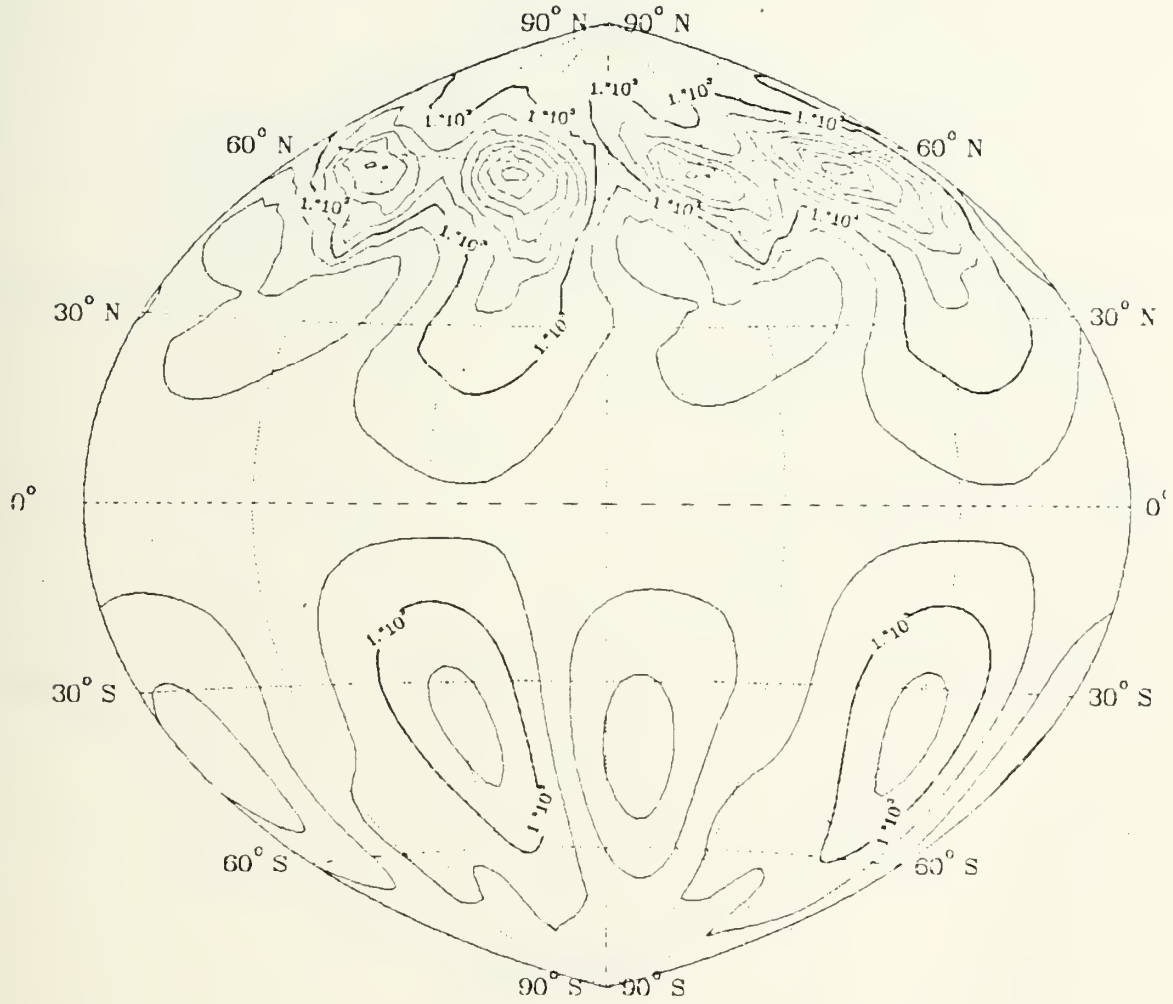

Figure 4.25. Sea-level pressure field at 48 h for Experiment III. Contour interval is 10 mb.

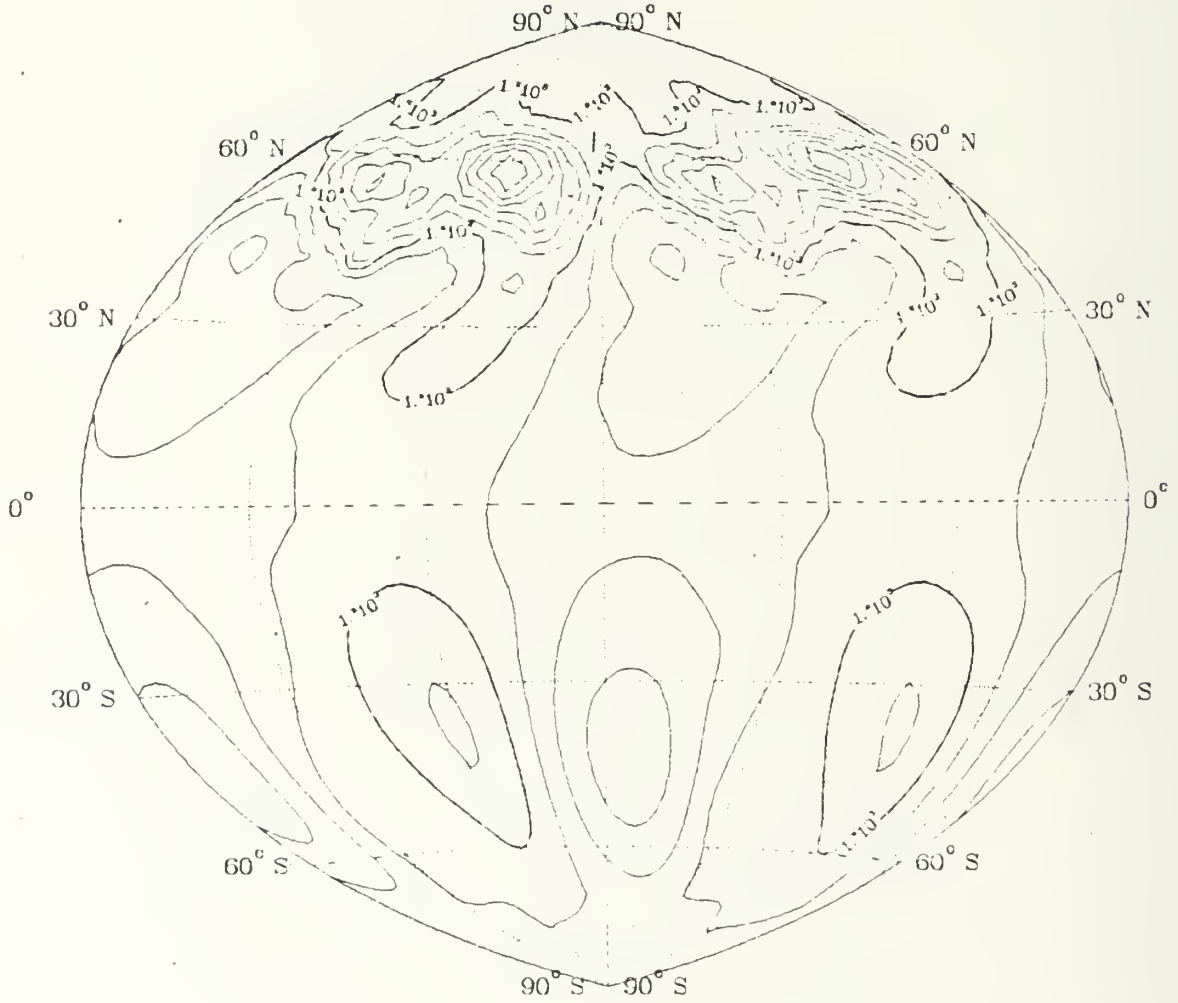

Figure 4.26. Sea-level pressure field at 54 h for Experiment III. Contour interval is 10 mb.

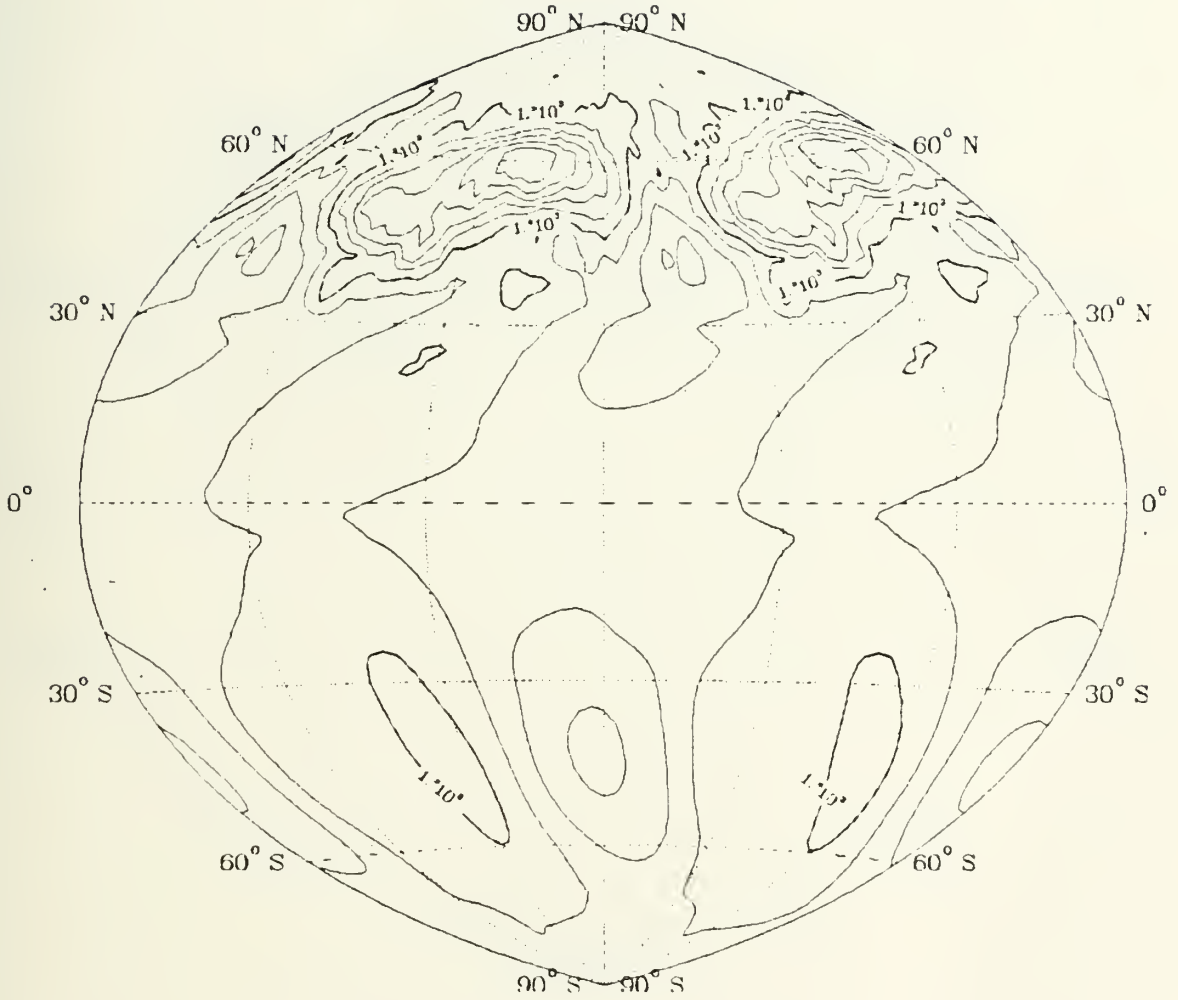

Figure 4.27. Sea-level pressure field at 66 h for Experiment III. Contour interval is 10 mb.

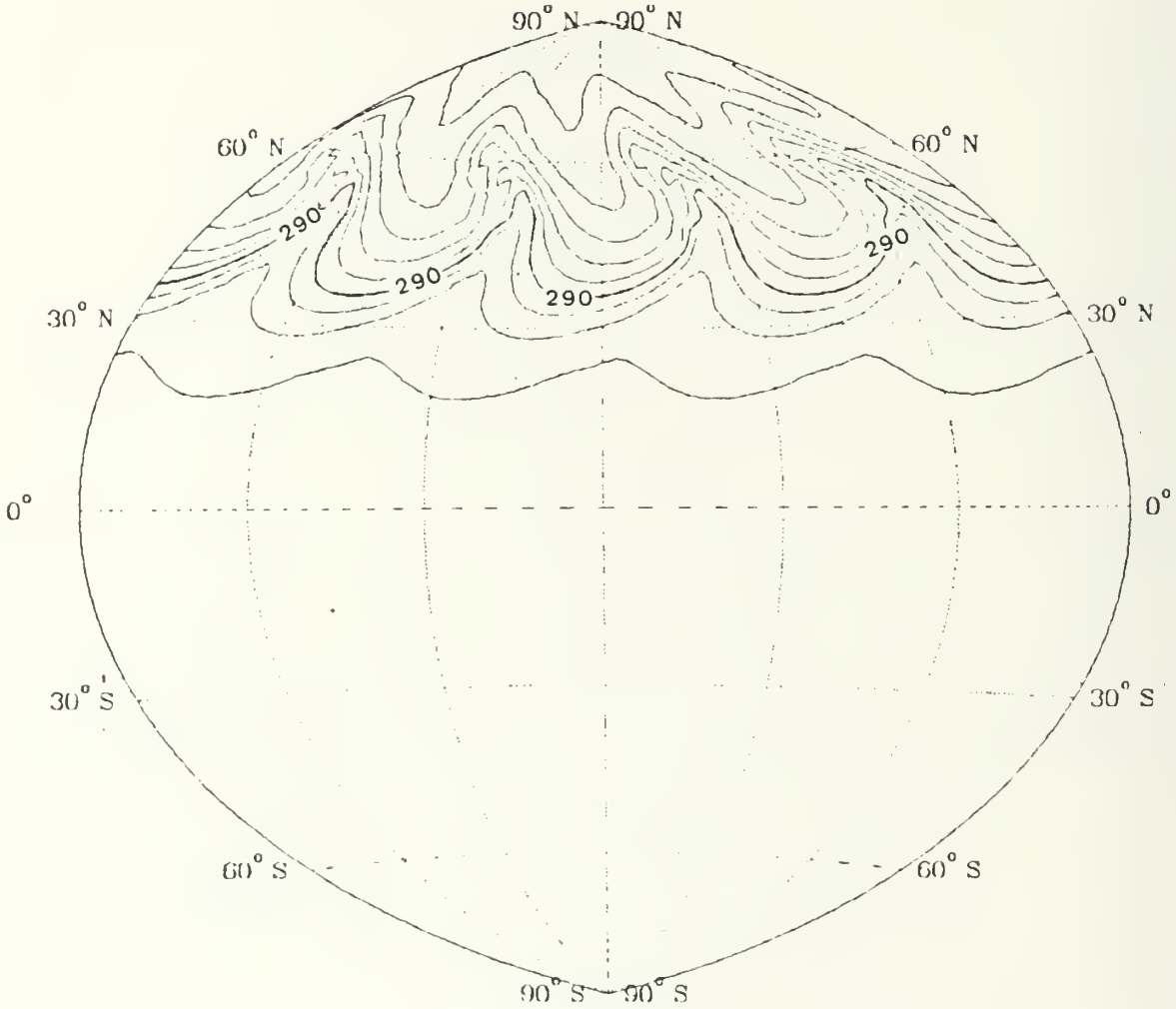

Figure 4.28. Potential temperature field at 36 h for Experiment III. Contour interval is 5° K.

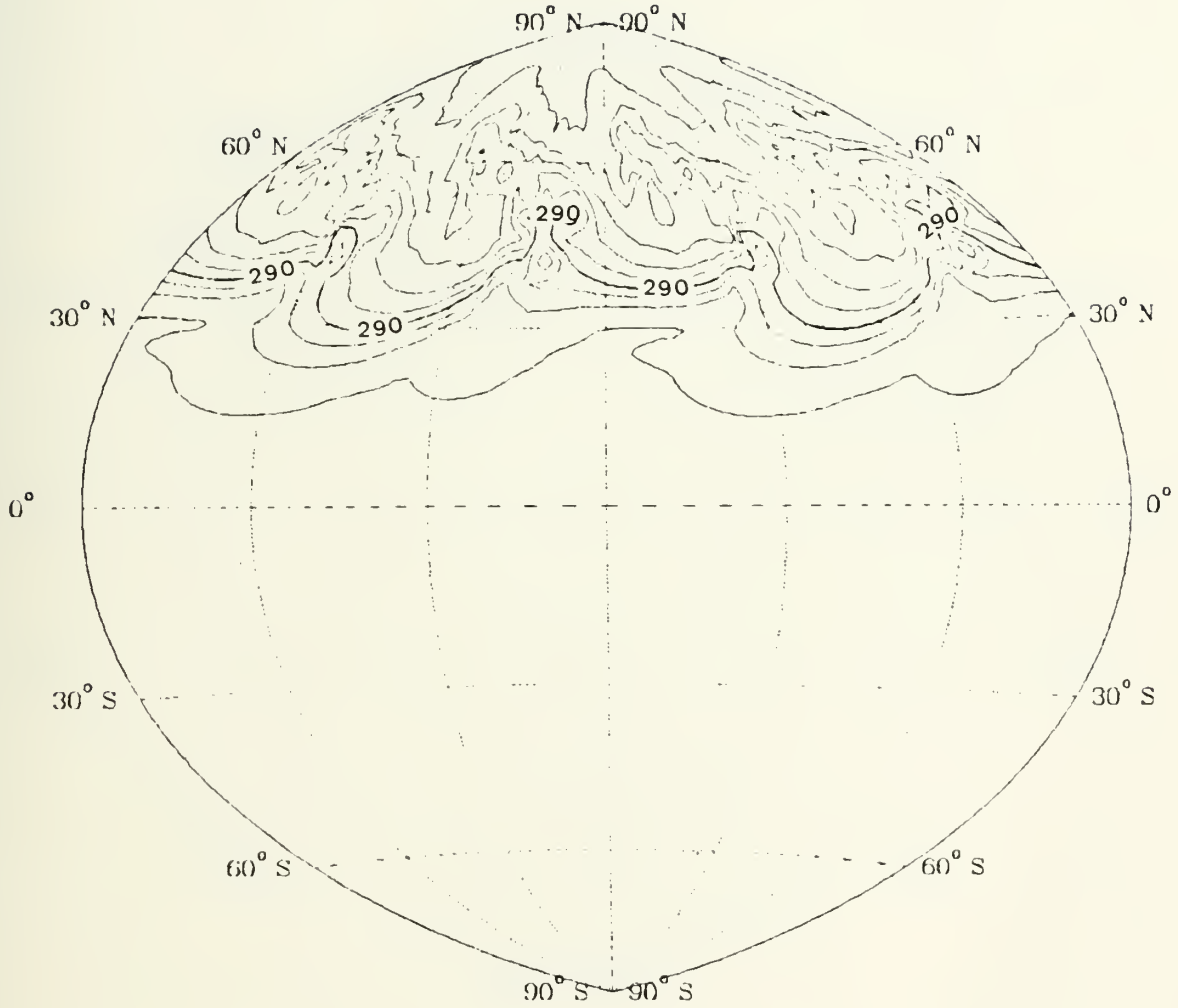

Figure 4.29. Potential temperature field at 48 h for Experiment III. Contour interval is 5° K.

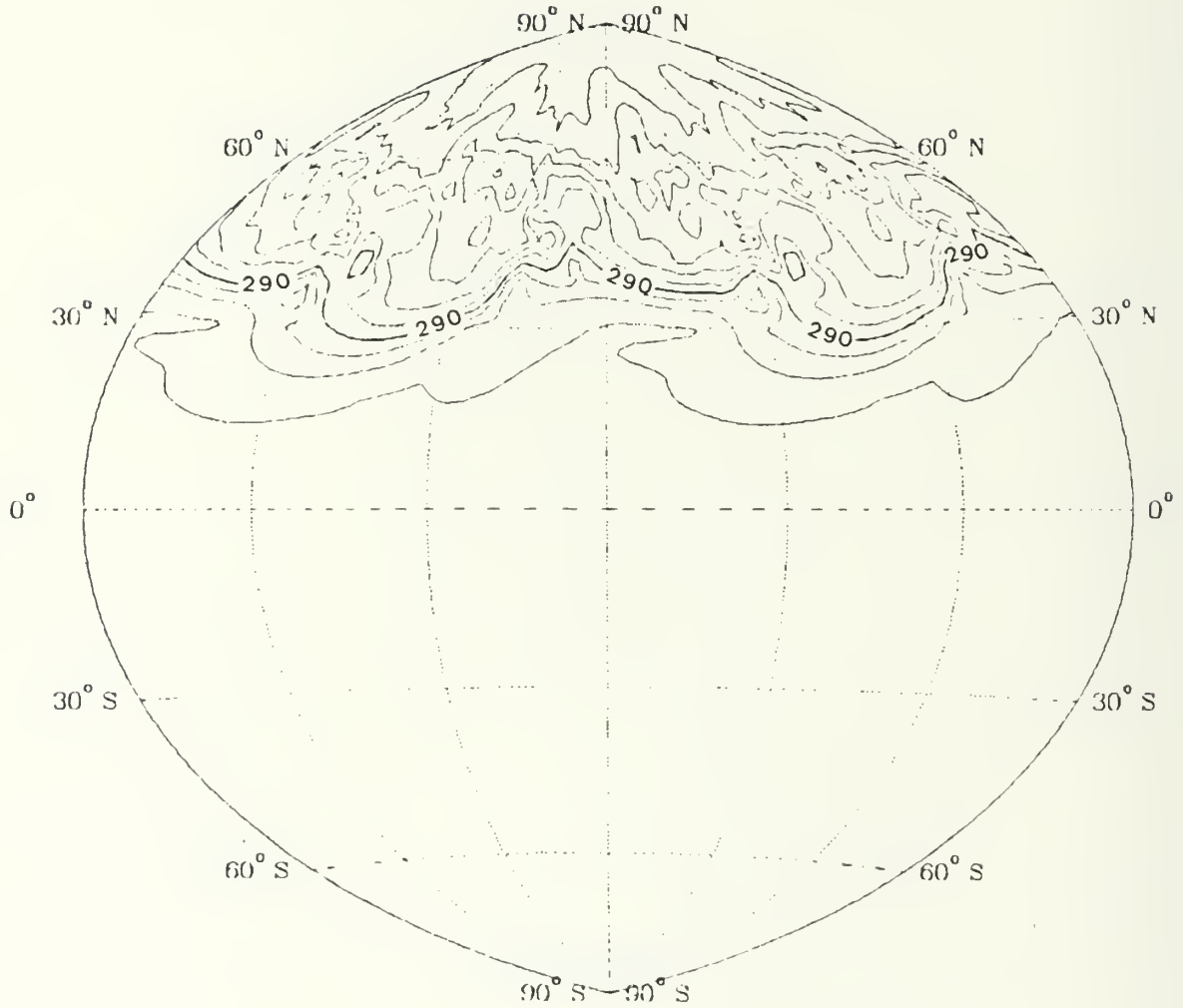

Figure 4.30. Potential temperature field at 54 h for Experiment III. Contour interval is 5° K.

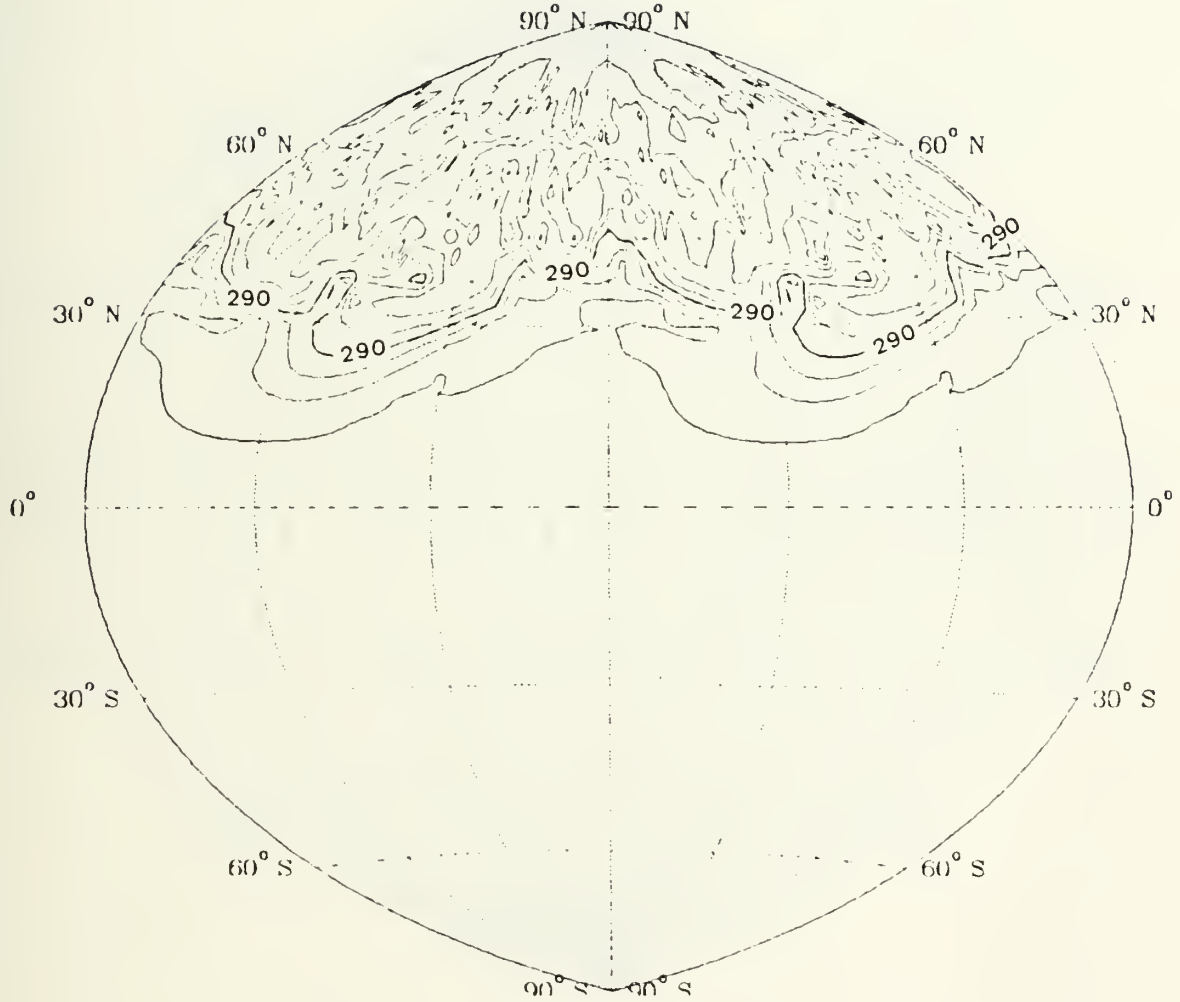

Figure 4.31. Potential temperature field at 66 h for Experiment III. Contour interval is 5° K.

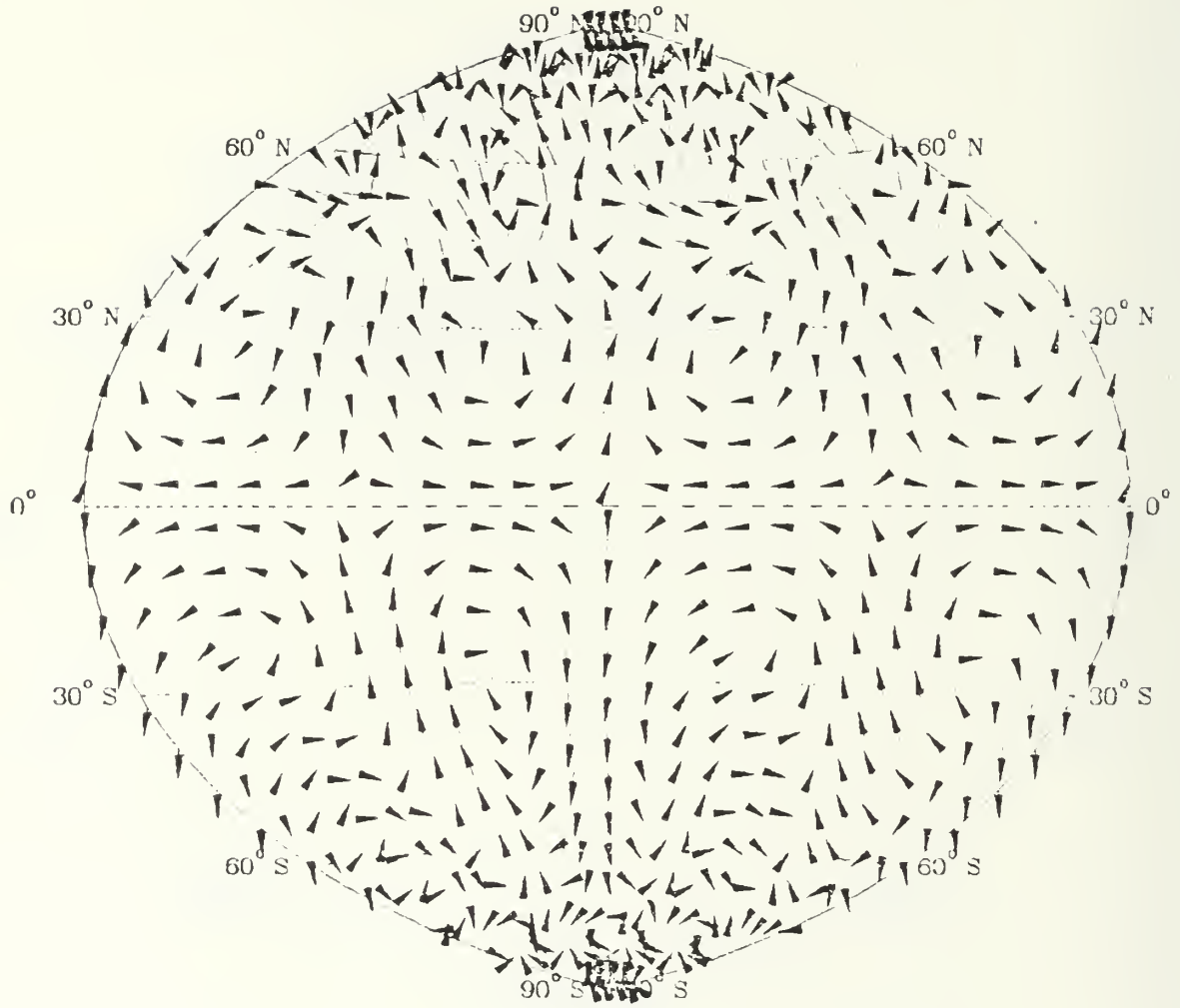

Figure 4.32. Wind vectors at 36 h for Experiment III. 4 mm = 20 m/s.

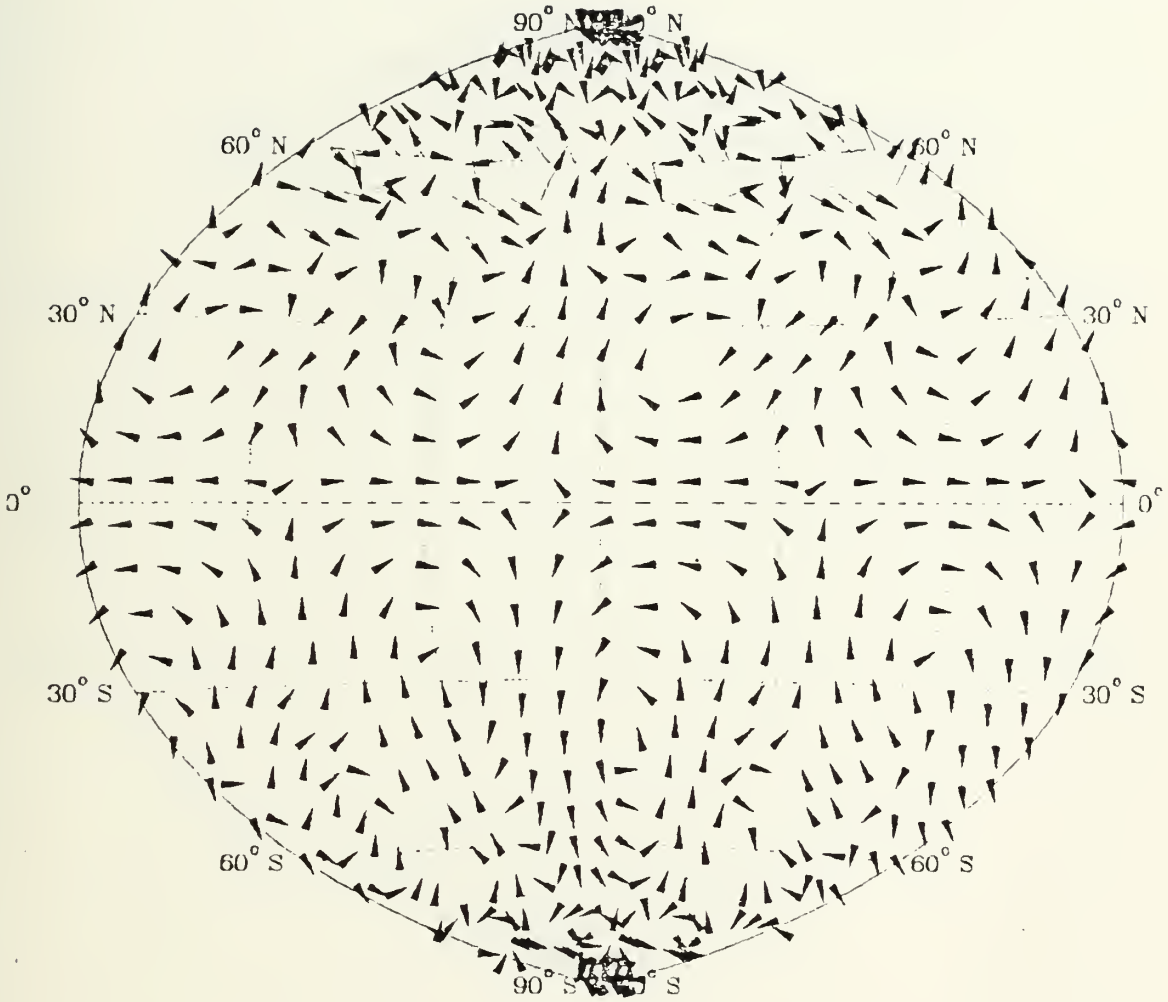

Figure 4.33. Wind vectors at 48 h for Experiment III. 8 mm = 50 m/s.

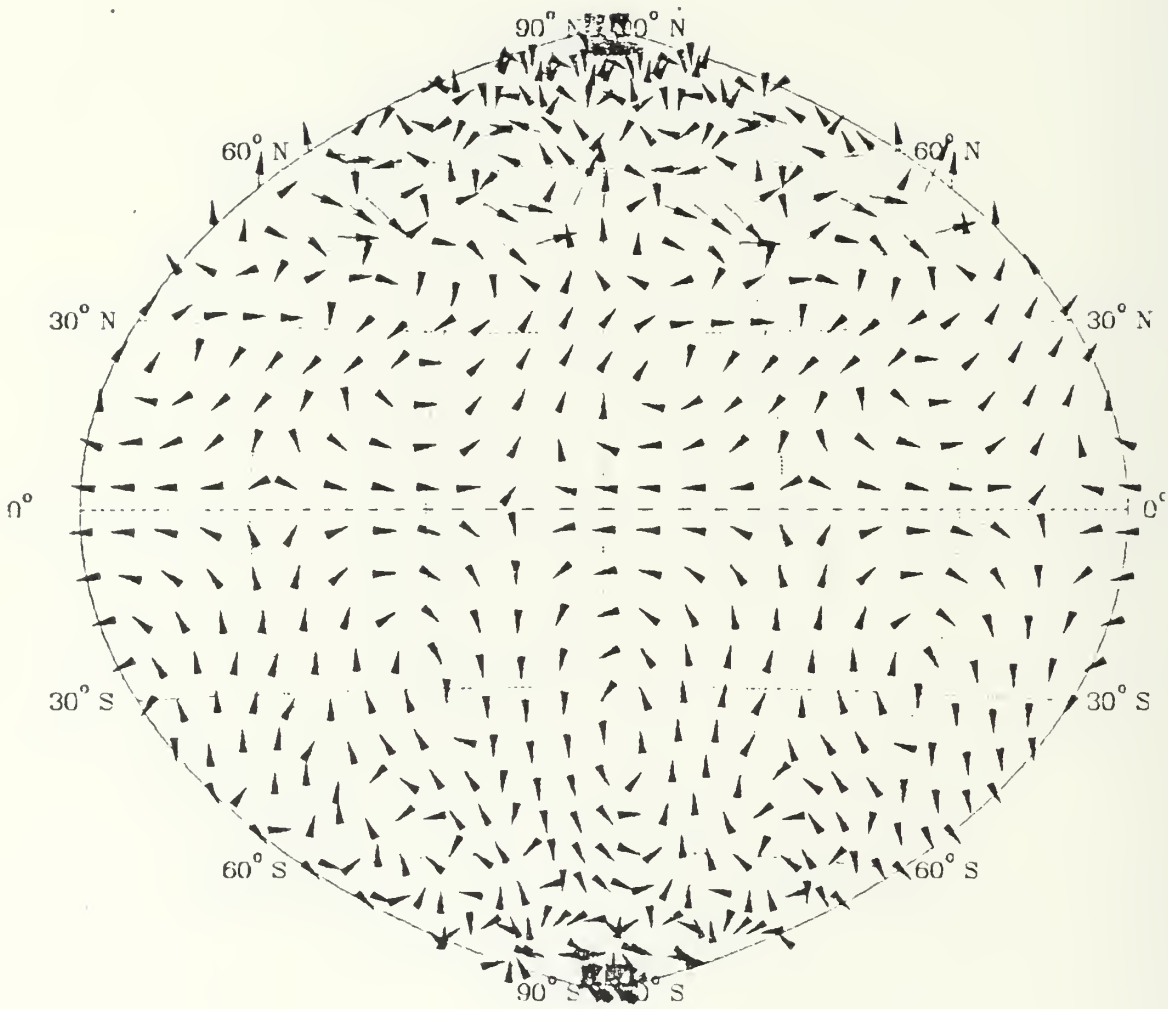

Figure 4.34. Wind vectors at 54 h for Experiment III. 8 mm = 50 m/s.

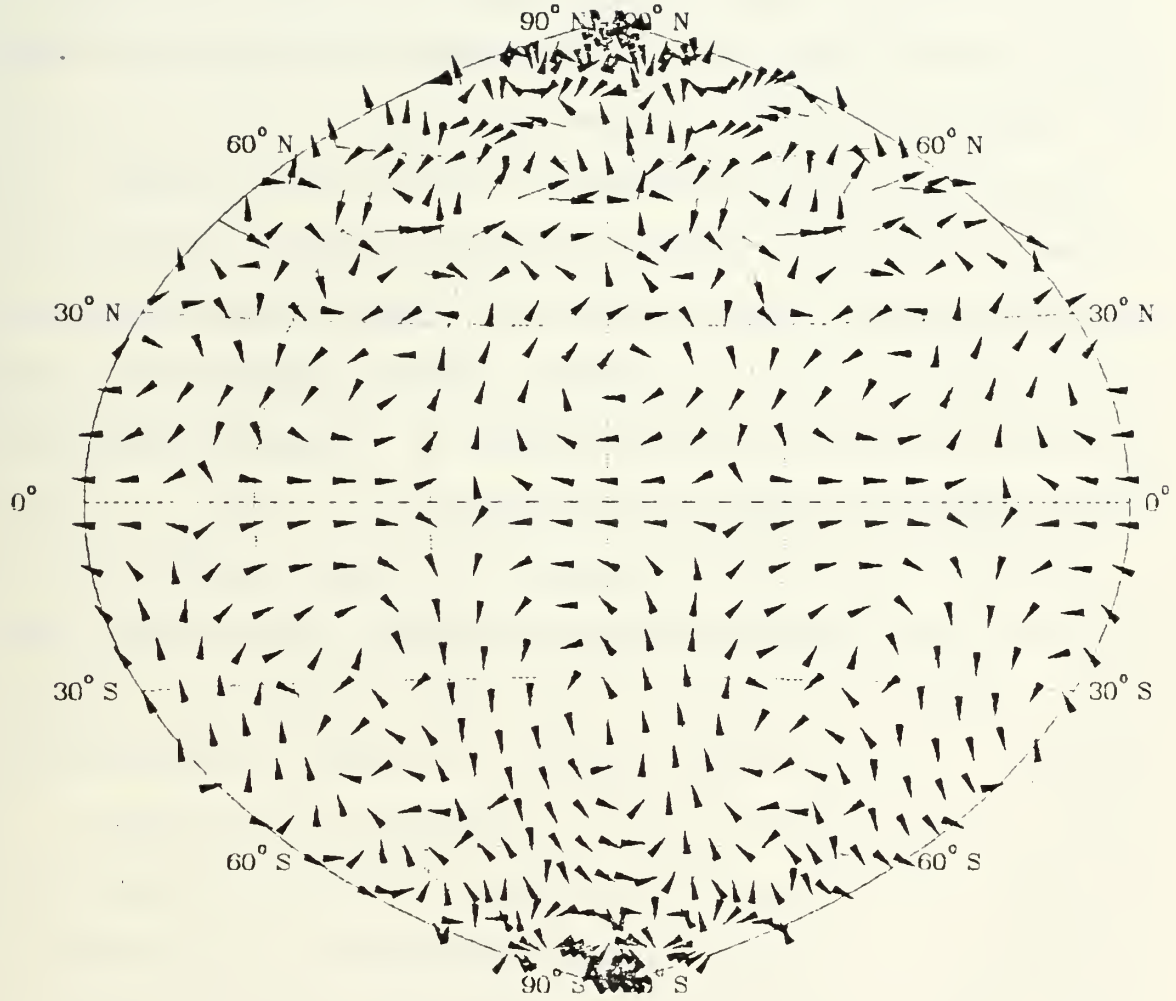

Figure 4.35. Wind vectors at 66 h for Experiment III. 8 mm = 50 m/s.

NE-SW. The small cyclone deepened at least 10 mb. The large cyclone deepened approximately 10 mb and moved slightly eastward with the mean flow. The tilting and weakening of the ridge caused three anticyclonic circulations to develop within the ridge particularly toward the northwest. At 48 h, winds are northeasterly from 40° N to about 10° N with a speed of at least 18 m/s.

The 48 h potential temperature field shows a broad tongue of cold air extending southwest near 20° N as if spreading over the South China Sea. The furthest extent is approximately 15° N. The thermal gradient remains weak south of 30° N and especially south of 20° N. A strong baroclinic zone is depicted behind the cold front.

Six hours later the secondary low pressure center is located 5° latitude further southeastward. The primary low center remained stationary. The ridge elongated and moved westward. This movement resulted in a band of northeasterly winds (of approximately 20 m/s) extending southwestward from 40° N to at least 10° N (Figure 4.34) as if along the eastern coast of China. These northeasterly winds advect colder temperatures as far south as 15° N (Figure 4.30). The strong baroclinic zone moved approximately 2.5° southeastward.

From 54 h to 66 h the low pressure center moves eastward, and the high pressure center moves westward. The pressure gradient south of 30° N decreases. The NE-SW

band of northeasterly winds narrowed but continues to advect cold temperatures as far south as approximately 10° N. The strong baroclinic zone continued moving southeastward but at a slower rate.

Several key observations are made based on this analysis. Northeasterly winds move rapidly south to the tropical regions in 12 h. These winds brought cold mid-latitude air to the tropics in 30 h. Compared to Experiment I, the northeasterly winds are stronger but do not go quite as far south into the equatorial region. The sea-level pressure pattern progresses eastward very little because additional forcing is necessary to overcome the beta effect on wave number 4. The pressure ridge and the cold air tongue are better defined than the wind surge. Baroclinic processes are present in the results of this experiment south of 30° N.

V. CONCLUSIONS

The interaction of a stable planetary wave with a growing cyclonic disturbance in a mid-latitude baroclinic flow was examined. The purpose of this study was to determine the contribution of a quasi-stationary stable wave number 4 to the initiation of a monsoon surge as a wave number 8 cyclone develops.

Several circulation features have been identified as characteristic of monsoon surges. They include: (1) the strengthening of north-northeasterly winds in the South China Sea, (2) a sharp drop in surface temperature at observation stations in China and Southeast Asia, (3) the shallow structure of the surge, (4) the strong baroclinic zone and (5) northerly winds in the tropics. In varying degrees, each of these characteristics were observed in one or more of the experiments.

In Experiment I, the jet provided enough additional forcing to the wave number 4 to produce cold temperatures and strong northerly winds in the tropics. The 305° K isotherm moved from near 10° N to south of the equator in 48 h. The winds were initially northerly with a small area of northeasterly winds. Throughout the experiment, the winds on the east side of the anticyclone became more northeasterly and increased in speed in the equatorial region. A strong baroclinic zone was observed on the downwind side of the trough.

Experiment II showed the evolution of an unstable baroclinic wave which was limited to the mid-latitudes. The 300° K isotherm moved south approximately 5° latitude in 48 h, as opposed to 10° and south of the equator in Experiment I. A strong baroclinic zone, which is characteristic of a frontal zone, was evident in the low-level potential temperature fields at the mid-latitudes, but it did not propagate southward into the tropics. In this experiment there were no significant northerly winds south of 45° N and no cold temperatures south of 30° N.

Several characteristics of monsoon surges were observed in Experiment III in which the wave number 4 and wave number 8 were combined. North-northeasterly winds reached the tropical regions 12 h after the addition of the long wave. Cold air moved southward to approximately 10° N within 30 h after the addition of the long wave. A strong baroclinic zone was evident in the potential temperature fields. It was advected southward to the tropics. Northerly winds were observed in the tropics at least as far south as 10° N. Experiment III roughly approximated events occurring during a cold surge.

These results suggest that the combination of quasi-stationary stable long wave and a developing mid-latitude cyclone initiate a monsoon surge. Additional forcing appears to be required to keep wave number 4 stationary. Wave number 4 also should be modified so that it does not extend to the

equator initially. Moving the jet and the maximum latitudinal amplitude of the perturbation to 35° N would increase the baroclinicity south of 30° N as well as more closely model the observed position of the jet during a surge event. This study found that a quasi-stationary stable wave number 4 and an unstable wave number 8 could initiate a monsoon surge.

APPENDIX A

MODEL PRIMITIVE EQUATIONS

Equation of State:

$$p\alpha = RT$$

Hydrostatic Equation:

$$\frac{\partial \phi}{\partial \sigma} = - \pi \alpha$$

Horizontal Momentum Equation:

$$\Pi\left(\frac{d\tilde{V}}{dt}\right) + f\,\tilde{k}\,\Pi\,\tilde{V} + \tilde{\nabla}_0(\Pi\Phi) - \tilde{\nabla}\,\Pi\frac{\partial(\Phi\sigma)}{\partial\sigma} = 0$$

Continuity Equation:

$$\frac{\partial \Pi}{\Pi t} + \tilde{\nabla}_0 \cdot (\Pi\tilde{V}) + \frac{\partial(\Pi\dot{\sigma})}{\partial\sigma} = 0$$

1st Law of Thermodynamics:

$$\frac{\partial(\Pi C_p \ell n\,\theta)}{\partial\sigma} + \tilde{\nabla}\cdot(\Pi\,\tilde{V} C_p \ell n\,\theta) + \frac{\partial(\Pi\dot{\sigma} C_p \ell n\,\theta)}{\partial\sigma} = 0$$

APPENDIX B

LIST OF SYMBOLS

A	constant
a	radius of the earth
C	constant
C_p	specific heat at constant pressure
f	Coriolis parameter
f_0	value of Coriolis parameter at 45° N
g	gravitational acceleration
m	wave number
p	pressure ($p = p + p' + P'$)
p_0	surface pressure at 45° N, 1013.25 mb
p_m	maximum model pressure height, 125 mb
p_s	surface pressure
p_t	pressure at tropopause
R	gas constant for air
S	smoothing operator
T	temperature
T_0	surface temperature at 45° N, 288° K
T_s	surface temperature
u	zonal velocity component ($u = u + u' + U'$)
u_m	maximum velocity, surface: 5 m/s, upper: 65 m/s
u_s	surface velocity component
u_u	upper level velocity component

v	meridional velocity component ($v = v + v' + V'$)
Z	terrain height
α	specific volume
β	frequency
γ	halfwidth of jet
Γ	dry adiabatic lapse rate, 6.5° K/km
θ	potential temperature
λ	longitude
π	3.14159
Π	normalized pressure
σ	vertical coordinate
$\dot{\sigma}$	vertical velocity in sigma coordinate system
ϕ	latitude
ϕ_0	latitude of jet
Φ	geopotential, also current terrain height
Ω	angular velocity of the earth
ω	angular velocity of air relative to the earth (mean flow)
ψ	stream function

LIST OF REFERENCES

Arakawa, A. and V. Lamb, 1977: Computational Design of the Basic Dynamical Processes of the UCLA General Circulation Model. Methods in Computational Physics, Vol. 17, Academic Press, 337 pp.

Arakawa, A. and V. Lamb, 1981: A Potential Enstrophy and Energy Conserving Scheme for the Shallow Water Equations. Mon. Wea. Rev., 109, 18-36.

Baker, B.J., 1983: Numerical Simulation of the Forcing of Monsoon Surges by Mid-Latitude Baroclinic Waves. Master's Thesis, Naval Postgraduate School, Monterey, CA, September 1983, 109 pp.

Chang, C.-P., G.T.J. Chen and J.E. Millard, 1983: Gravitational Characgerif Cold Surges during Winter MONEX. Mon. Wea. Rev., 111, 293-307.

Chang, C.-P., J.E. Erickson and K.M.W. Lau, 1979: Northeasterly Cold Surges and Near-Equatorial Disturbances over the Winter MONEX Area during December 1974. Part I: Synoptic Aspects. Mon. Wea. Rev., 107, 812-829.

Chang, C.-P. and K.M.W. Lau, 1980: Northeasterly Cold Surges and Near-Equatorial Disturbances over the Winter MONEX Area during December 1974. Part II: Planetary-Scale Aspects. Mon. Wea. Rev., 108, 298-312.

Chang, C.-P. and K.M.W. Lau, 1982: Short-Term Planetary-Scale Interactions over the Tropics and Midlatitudes during Northern Winter. Part I: Contrasts between Active and Inactive Periods. Mon. Wea. Rev., 110, 933-946.

Chu, E.W.K., 1978: A Method for Forecasting the Arrival of Cold Surges in Hong Kong. Royal Observatory Technical Note No. 43, 31 pp.

Danielson, E.F. and F.P. Ho, 1969: An Isentropic Trajectory Study of a Strong Northeast Monsoon Surge. Air Force Cambridge Research Laboratories, Report No. 69-0036, 13 pp.

Haltiner, G.J. and R.T. Williams, 1980: Numerical Weather Prediction and Dynamic Meteorology. John Wiley and Sons, 477 pp.

Haurwitz, B., 1940: The Motion of Atmospheric Disturbances on the Spherical Earth. J. Marine Research, 3, 254-267.

Hayes, J.L., 1985: A Numerical and Analytical Investigation of Lee Cyclogenesis. Ph.D. Thesis, Naval Postgraduate School, Monterey, CA, March 1985. 138 pp.

Lim, H. and C.-P. Chang, 1981: A Theory for Midlatitude Forcing of Tropical Motions during Winter Monsoons. J. Atmos. Sci., 38, 2377-2392.

Murakami, T., 1979: Winter Monsoon Surges over East and Southeast Asia. J. Meteor. Soc. Japan, 57, 133-158.

Ramage, C.S., 1971: Monsoon Meteorology. Academic Press, 296 pp.

Shaffer, A.R., C.-P. Chang and R.L. Elsberry, 1984: Long-wave Forcing of Equatorial Penetrating Winter Monsoon Cold Surges. Preprints: 15th Conference on Hurricanes and Tropical Meteorology (Miami, Florida), Amer. Meteor. Soc., Boston, 427-432.

INITIAL DISTRIBUTION LIST

		No. Copies
1.	Defense Technical Information Center Cameron Station Alexandria, Virginia 22304-6145	2
2.	Library, Code 0142 Naval Postgraduate School Monterey, California 93943-5100	2
3.	Commander Naval Oceanography Command NSTL Station Bay St. Louis, Missouri 39522	1
4.	Commanding Officer Fleet Numerical Oceanography Center Monterey, California 93943	1
5.	Commanding Officer Air Force Global Weather Center Offutt Air Force Base, Nebraska 68113	1
6.	Officer-in-Charge Naval Environmental Prediction Research Facility Monterey, California 93943	1
7.	Prof. R.J. Renard, Code 63Rd Naval Postgraduate School Monterey, California 93943-5100	1
8.	Lt. Col J. Cipriano AFIT/CIRF Wright-Patterson AFB, Ohio 45433	1
9.	Air Weather Service Technical Library Scot AFB, Illinois 62225	1
10.	Captain Nancy E. Harris USAF Environmental Technical Applications Center/DNY Scott AFB, Illinois 62225	2
11.	Prof. R.T. Williams, Code 62Wu Naval Postgraduate School Monterey, California 93943-5100	3

12. Dr. M.A. Rennick, Code 63 — 1
Naval Postgraduate School
Monterey, California 93943-5100

13. Prof. C.P. Chang, Code 63Cp — 1
Naval Postgraduate School
Monterey, California 93943-5100

14. Prof. R.L. Elsberry, Code 63Es — 1
Naval Postgraduate School
Monterey, California 93943-5100

15. Dr. T. Rosmond — 1
Naval Environmental Prediction
Research Facility
Monterey, California 93943

16. Dr. J. Hovermale — 1
Naval Environmental Prediction
Research Facility
Monterey, California 93943

17. Prof. C.H. Wash, Code 63 — 1
Naval Postgraduate School
Monterey, California 93943-5100

18. Captain A.R. Shaffer — 1
Det 1, 2 WS
Wright-Patterson AFB, Ohio 45433

19. Dr. A. Arakawa — 1
Department of Meteorology
University of California
Los Angeles, California 90024

20. Dr. A. Kasahara — 1
National Center for Atmospheric Research
P.O. Box 3000
Boulder, Colorado 80303

21. Prof. N.A. Phillips — 1
National Meteorological Center/NOAA
World Weather Building
Washington, D.C. 20233

22. Dr. J. Young — 1
Department of Meteorology
University of Wisconsin
Madison, Wisconsin 53706

23. Major John L. Hayes 1
HQ AWS/DNXP
Scott AFB, Illinois 62225

24. Commander Carl Ihli 1
C.O. NOCF
San Diego, California 92152

25. Professor Hock Lim 1
Blk 1M Prine Grove
#01-46
Singapore 2159
Republic of Singapore

26. Professor G.T. Chen 1
Dept. of Atmospheric Sciences
National Taiwan University
Taipei, TAIWAN 107
R.O.C.

214289

Thesis
H291263 Harris
c.1 Numerical simulation of cold surges.